A Scheme for Representing Cumulus Convection in Large-Scale Models

KERRY A. EMANUEL

Center for Meteorology and Physical Oceanography, Massachusetts Institute of Technology, Cambridge, Massachusetts

(Manuscript received 11 April 1990, in final form 10 April 1991)

ABSTRACT

Observations of individual convective clouds reveal an extraordinary degree of inhomogeneity, with much of the vertical transport accomplished by subcloud-scale drafts. In view of these observations, a representation of moist convective transports for use in large-scale models is constructed, in which the fundamental entities are these subcloud-scale drafts rather than the clouds themselves. The transport by these small-scale drafts is idealized as follows. Air from the subcloud layer is lifted to each level i between cloud base and the level of neutral buoyancy for undilute air. A fraction (ϵ^i) of the condensed water is then converted to precipitation, which falls and partially or completely evaporates in an unsaturated downdraft. The remaining cloudy air is then assumed to form a uniform spectrum of mixtures with environmental air at level i; these mixtures ascend or descend according to their buoyancy.

The updraft mass fluxes M^i are represented as vertical velocities determined by the amount of convective available potential energy for undilute ascent to level i, multiplied by fractional areas σ^i, which are in turn determined in such a way as to drive the mass fluxes toward a state of quasi-equilibrium with the large-scale forcing. The downdraft mass fluxes are unique functions of the M^i, so that determination of the M^i closes the system.

The main closure parameters in this scheme are the *parcel precipitation efficiencies*, ϵ^i, which determine the fraction of condensed water in a parcel lifted to level i that is converted to precipitation, and the fraction σ_i^s of precipitation that falls through unsaturated air. These may be specified as functions of altitude, temperature, adiabatic water content, and so on, and are regarded as explicitly determined by cloud microphysical processes. Specification of these parameters determines the vertical profiles of heating and moistening by cloud processes, given the large-scale (explicitly resolved) forcing. It is argued here that accurate calculation of the moistening by cumulus clouds cannot proceed without addressing the microphysics of precipitation formation, fallout, and reevaporation.

One-dimensional radiative–convective equilibrium experiments with this scheme produce reasonable profiles of buoyancy and relative humidity. When large-scale descent is imposed, a trade-cumulus regime is produced, including a trade inversion and mixing-line structure in the cloud layer.

1. Introduction

When the virtual temperature lapse rate within numerical models of the atmosphere becomes superadiabatic, it is adjusted back to its adiabatic value. This is done with very little ceremony or controversy because the twin principles of entropy conservation and convective neutrality uniquely determine the virtual temperature of the atmosphere after the adjustment.

When the atmosphere is unstable to moist convection, however, the problem is far more involved and controversial. In the first place, it is not generally agreed that the adjusted state is convectively neutral, although Betts (1982) and Xu and Emanuel (1988) argue that the tropical atmosphere is, on the average, neutral to reversible displacements (including adiabatic condensate loading) of subcloud-layer air.

Even if it could be asserted that the adjusted state is neutral, this alone does not determine the virtual temperature since entropy is not conserved during the adjustment; rather, it is increased by net condensation of water vapor. The increase of vertically integrated entropy depends on how much of the condensed water reaches the ground as precipitation.

To add to this problem, the water vapor distribution of the adjusted state is not known for either dry or saturated convective adjustment. To illustrate this point, consider an atmosphere in radiative-moist convective equilibrium. The mass flux in clouds must be such that the associated environmental subsidence warming exactly balances radiative cooling; thus, if the latter is known, the former is easily determined. But the flux of water substance by the clouds depends not only on the vapor flux, which is known since the cloud air is saturated, but also on the flux of condensed water, which is strongly influenced by precipitation fallout. Thus, the equilibrium water vapor content of the environment depends sensitively on the processes that determine the amount of cloud water remaining in de-

Corresponding author address: Professor Kerry Emanuel, Building 54-1620, Center for Meteorology and Physical Oceanography, MIT, Cambridge, MA 02139.

training air. In problems such as global climate, it is crucial to predict correctly the distribution of water vapor, the most important greenhouse gas (Lindzen 1990). The distribution of moistening by convection also affects the formation of layered clouds, such as cirrus, which are of profound importance in the radiation budget of the earth.

An unavoidable consequence of these arguments is that both the heating and moistening of the atmosphere by convection depend on the details of how water is condensed, precipitated, and transported within convective clouds. Many existing representations of convective processes used in large-scale models avoid addressing the details of such processes by making sweeping assumptions about the distributions of moistening and/or heating by clouds. The adjustable parameters related to these distributions tend to be far removed from measurable properties of cumulus clouds, and validation of the schemes generally involves comparison of predicted and observed precipitation rates. Such comparisons are problematic because they validate only the vertical integrals of moistening and heating and not their distributions. Moreover, the vertical distribution of heating is an exceedingly poor validation field for convective schemes because this is determined almost entirely by the large-scale profile of adiabatic and radiative cooling, which together balance almost all of the convective heating.

In view of the preceding, I argue that an effective representation of convection must be built solidly on the physics and microphysics of cloud processes as deduced from observations, numerical cloud models, and theory. This paper describes an attempt to construct a convective representation based on recent observations and theory of convective clouds. The following section reviews the observational basis of the current understanding of convective clouds. Section 3 describes the convective representation itself, and the results of applying this representation to simple one-dimensional equilibrium states are presented in section 4. Section 5 compares the present scheme with others in current use, and section 6 presents a concluding discussion.

2. Observational basis

a. Mixing in clouds

Detailed aircraft measurements of the structure of ordinary cumulus clouds date back to the work of Stommel (1947), Malkus (1954), Warner (1955), and Warner and Squires (1958). These observations invariably show that the fluctuations of vertical velocity inside such clouds are much larger than the velocity horizontally averaged across the cloud. Temperature, water vapor, and liquid water content are also highly variable, with important structure on the 100-m scale.

In 1958 Squires pointed out that the turbulent mixing of dry environmental air near the tops of clouds produces substantial negative buoyancy, leading to a phenomenon he called penetrative downdrafts. [These were subsequently shown by Emanuel (1981) to be potentially as strong as or stronger than convective updrafts.] The importance of such drafts was emphasized by Telford (1975) and Raymond (1979), and by Warner (1970), who pointed out that mixing by penetrative downdrafts could explain some of the discrepancies between real clouds and those modeled as simple entraining plumes.

The first concrete observational evidence of the occurrence of penetrative downdrafts was presented by Paluch (1979), who used the conserved variables θ_e (equivalent potential temperature) and Q (total water mixing ratio) to deduce the environmental origin of air sampled by gliders inside Colorado cumuli. She showed that the interiors of nonprecipitating cumuli were extremely inhomogeneous, with some samples representing nearly undilute ascent from cloud base and others exhibiting various mixtures of subcloud air with environmental air from near the tops of the clouds. She saw little evidence of lateral entrainment. Subsequent work by Boatman and Auer (1983), Jensen et al. (1985), and LaMontagne and Telford (1983) appears to support the conclusions of Paluch (1979), but recent work by Blyth et al. (1988), Raga et al. (1990), and Taylor and Baker (1991) suggests that lateral entrainment occurs as well. The relative importance of these two entrainment mechanisms has not been firmly established, except in a limited number of cases, and probably depends on the size and age of the cloud and the character of the environment.

These observations cast serious doubts on the validity of treating clouds themselves as bulk-entraining plumes. Already in 1970 Warner pointed out that entraining plume models could not simultaneously predict the cloud top height and liquid water content of observed clouds; if the entrainment rate is adjusted to predict the observed height, then the liquid water contents are much too high. The entraining plume model rests on the assumption that entrained environmental air is immediately homogenized with the cloud so that the latter can be characterized by single values of buoyancy and liquid water at each altitude.

At the opposite extreme is the idea first advanced by Telford (1975) that individual subcloud-scale parcels of air ultimately arrive at their individual levels of neutral buoyancy, so that a single "cloud" may detrain at multiple levels. Such a model can explain why some air from the subcloud layer can rise nearly undiluted by entrainment, so that the cloud top is at the undilute level of neutral buoyancy (as generally observed), while most of the air mixes with the environment and detrains at lower levels. The model thus potentially resolves the liquid water–cloud top paradox raised by Warner (1970). Since Telford advanced his hypothesis, considerable observational evidence has been amassed in its favor. Raymond and Wilkening (1982, 1985) conducted experiments in which New Mexico cumuli

were circumnavigated by aircraft at different levels so that the net mass flux in and out of the clouds could be deduced. Their results show strong middle-level outflow, with net mass inflow into the bases and tops of the clouds, implying net downward motion near the cloud tops. Most recently, a study of trade wind cumuli near Hawaii by Raga et al. (1990) shows that while the vertical mass flux is upward through most of the cloud layer, descent occurs near the cloud top at the altitude of the trade inversion.

It seems inevitable that individual air parcels involved in convection will ultimately attain a state of neutral buoyancy with respect to their environments. What remains unclear is the exact nature of the turbulent mixing that occurs among different samples of air en route to buoyant equilibrium. The entraining plume model assumes that subcloud-layer air is continually and thoroughly mixed with the clear environment on its ascent. At the opposite extreme is the stochastic model of Raymond and Blyth (1986), which assumes that individual subcloud-layer air parcels undergo only one mixing event on their way to neutral equilibrium. The problem with this hypothesis, as pointed out by Taylor and Baker (1991), is that cloudy air detrained at its level of neutral buoyancy will become negatively buoyant on mixing with its subsaturated environment. What one seeks here is a model that predicts where air will ultimately detrain. But the idea of buoyancy sorting is receiving increasing confirmation by observations, most recently those of Taylor and Baker (1991). It is that idea upon which the present scheme is based.

b. *Precipitation-driven downdrafts*

Convecting atmospheres usually exhibit a strong upward decrease of θ_e in the lower troposphere. The low θ_e of the middle troposphere affords a large potential for downdrafts driven by the evaporation of precipitation that falls into the dry air from a cloud. The rain may fall directly from sloping convective towers (LeMone et al. 1984) or from the anvils of tall convective clouds or cloud complexes (Zipser 1969; Houze 1977). The thermodynamic effects of such downdrafts are very large, so much so that the cooling may more than cancel convective heating in the lower troposphere (e.g., see Houze 1989). To the casual observer, the cold rush of air that precedes thunderstorms at the surface is perhaps their most obvious manifestation. There is increasing evidence that such downdrafts play a decisive role in organizing squall lines (Zipser 1969; Houze 1977; Seitter and Kuo 1983; Rotunno et al. 1988), and perhaps other forms of mesoscale convective systems. Since these downdrafts transport low-entropy (θ_e) air into the boundary layer, they constitute an important means by which convection stabilizes the atmosphere. Recently, the author (Emanuel 1989) argued that convective downdrafts are responsible for preventing the spontaneous genesis of tropical cyclones over warm oceans.

It seems improbable that a successful representation of convection can be formulated without accounting for the effects of unsaturated downdrafts.

3. The model

a. *Saturated updrafts and downdrafts*

In view of the observations discussed in the preceding section, I formulate here a representation of convective fluxes based on an idealized model of subcloud-scale updrafts and downdrafts. It is important to note that I am explicitly attempting to represent the collective effects of an ensemble of individual, O(100 m)-scale drafts, not of ensembles of O(1 km)-scale clouds. These drafts, rather than whole clouds, are regarded as the fundamental agents of convective transport.

The idealization of the convective process is illustrated in Fig. 1, and is based on the models of Raymond and Blyth (1986) and Telford (1975) and on the aforementioned observations. I take as a starting point the vertical thermodynamic structure of the atmosphere. The level of cloud base (ICB) and the first level of neutral buoyancy (INB) for the undilute, reversible ascent of near-surface air are first determined from the sounding. If the latter is at a higher altitude than the former, convection is assumed to occur.

For simplicity, I will regard the atmosphere as consisting of a finite number of discrete layers, each associated with a temperature, water vapor mixing ratio, and pressure, anticipating that most implementations of a convective representation will be in the context of models whose vertical structure is phrased in finite-difference equations.

Suppose air is lifted without mixing from the subcloud layer to an arbitrary level i between cloud base and cloud top (ICB $< i \leqslant$ INB). We now allow a specified fraction, ϵ^i, of the condensed water to be converted into precipitation, leaving an amount of cloud water l_c^i given by

$$l_c^i = (1 - \epsilon^i) l_a^i, \tag{1}$$

where l_c^i is the cloud water mixing ratio at level i and l_a^i is the adiabatic water content at that level. The disposition of the precipitation will be dealt with in section 3b.

The cloudy air is next mixed with its environment at level i. Lacking information to the contrary, I assume an equal probability distribution of the mixing fraction, σ^i, following Raymond and Blyth (1986). Each mixture then ascends or descends to its new level of neutral buoyancy.

In the Raymond and Blyth model, the air then detrains at its new level of neutral buoyancy. But as mentioned above, if the neutrally buoyant mixture is cloudy, it will usually become negatively buoyant on

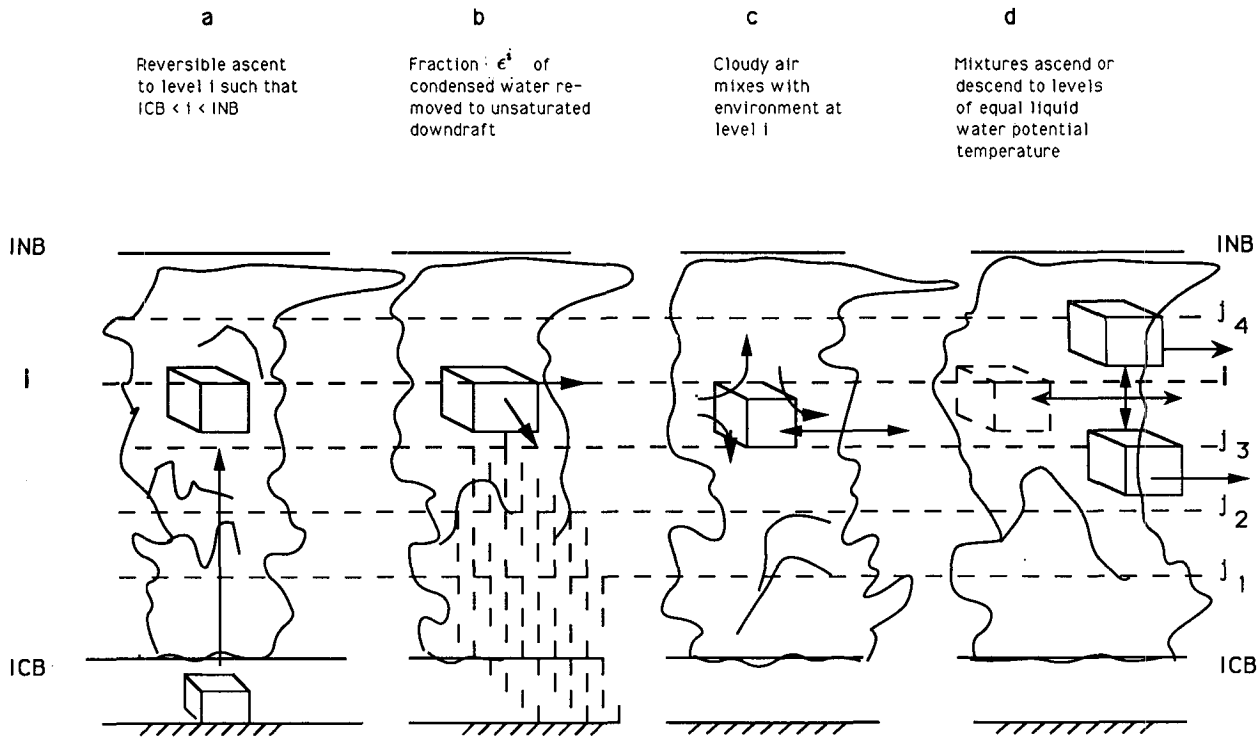

FIG. 1. Idealized model of the convection of subcloud-scale parcels. (a) Reversible ascent from subcloud layer to arbitrary level (i) between cloud base (ICB) and level of neutral buoyancy (INB). (b) A fraction ϵ^i of condensed water is converted to precipitation, which is added to a single unsaturated downdraft. (c) Remaining cloudy air is mixed according to an equal probability distribution with the environment at level i. (d) Mixtures then ascend or descend to levels at which their liquid water potential temperature is equal to that of their environment.

mixing with its new environment. It seems likely, as pointed out by Taylor and Baker (1991), that mixing will again take place and the new mixtures will once again proceed to their new levels of neutral buoyancy. This process may ultimately involve many "episodes" of mixing, as illustrated in Fig. 2.

As a strictly practical matter, it is necessary to truncate this process at some level in formulating a convective scheme. In climate models in particular it would appear to be impractical to proceed beyond the first buoyancy sorting, that is, beyond the level envisioned by Raymond and Blyth (1986). To avoid the problem mentioned by Taylor and Baker (1991), however, I will insist that the mixed air detrain only at levels at which *further* mixing with the environment will result in neutral buoyancy. This is equivalent to assuming that the mixtures detrain at levels at which their liquid water potential temperature, rather than their actual potential temperature, equals that of their environment. While somewhat unphysical, it will be apparent in actual practice that little if any cloud water remains in mixed parcels (see section 4).

The buoyancy-sorting tree used in the present scheme is illustrated in Figs. 1 and 2. The rate of mass flux from the subcloud layer to level i is M^i and is determined by a procedure to be discussed presently. A fraction ϵ^i of the condensed water is removed, as discussed previously. At level i, a number j of fractions σ^{ij} of environmental air at level i is mixed into the parcel according to an assumed equal probability distribution. If the mixture has a liquid water potential temperature, θ_l^{ij}, less than the potential temperature of its environment, it descends to a level j at which $\theta_l^{ij} = \theta^j$. No *new* precipitation formation is allowed since the condensed water content will decrease, perhaps to zero, during the downward displacement. If the mixture is such that $\theta_l^{ij} = \theta^i$, the mixed air is assumed to detrain at level i, again without further precipitation formation. If $\theta_l^{ij} > \theta^i$, however, the mixture is assumed to ascend to a new level j such that $\theta_l^{ij} = \theta^j$ *after* more precipitation is removed, according to

$$l^{ij}_{\text{new}} = l^{ij}(1 - \epsilon^j),$$

where l^{ij} is the condensed water content of the mixture.

The assumption of detrainment at levels of equal θ_l is unphysical, but avoids the problem of detraining air that would become negatively buoyant on further mixing. Moreover, the problem will usually be slight in practice, since descending air will usually have small or zero condensed water content, while ascending mixtures are assumed to have more condensed water re-

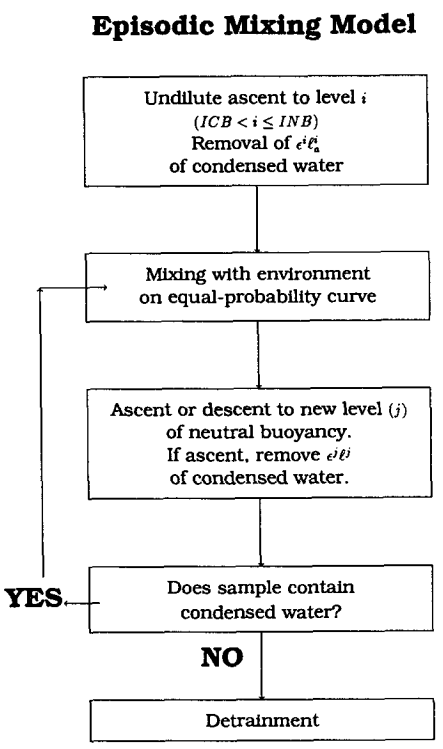

FIG. 2. Flow chart for episodic mixing model.

moved by precipitation. In the control simulation described in section 4, for example, none of the detraining *mixed* air is found to contain any condensed water. The method proposed appears to be the best way to truncate a series of discrete mixing events.

Ignoring the entropy of mixing, we may determine the liquid water potential temperature of a mixture created at level i and displaced to level j by first displacing the unmixed cloud from level i to level j and likewise displacing the unmixed environment from level i to level j, and *then* mixing (it may be mixed first instead, but this proves to be less convenient for numerical reasons). If σ^{ij} is the fraction of environmental air in the mixture, then the θ_l of the mixture at level j is

$$\theta_{lm}^{ij} = \sigma^{ij}\theta_l^{ij} + (1 - \sigma^{ij})\theta_{lp}^{ij}, \tag{2}$$

where θ_l^{ij} is the θ_l of the environment after being lifted to level j and θ_{lp}^{ij} is the θ_l of subcloud air after first being lifted to level i, depleted of water by precipitation, and then displaced to level j with further removal of precipitation if $j > i$. Thus if θ_{lp}^{i} is the θ_l of subcloud-layer air lifted to level i with removal of precipitation, then

$$\theta_{lp}^{i} = \theta_p \exp\left[\frac{\epsilon^i L_v l_a^i}{C_p T^i}\right], \tag{3}$$

where θ_p is the potential temperature of subcloud air, and L_v and C_p are the heat of vaporization and heat capacity of air at constant pressure, respectively. When this air is further displaced to level j, its θ_l will be given by

$$\theta_{lp}^{ij} = \begin{cases} \theta_{lp}^{i} \exp\left[\dfrac{\epsilon^j L_v l_p^{ij}}{C_p T^j}\right], & j > i \\ \theta_{lpi}, & j \leqslant i, \end{cases} \tag{4}$$

where l_p^{ij} is the condensed water produced in displacing the air adiabatically to level j. The θ_l of environmental air displaced adiabatically from level i to level j is

$$\theta_l^{ij} = \theta^i \exp\left[\frac{\epsilon^j L_v l^{ij}}{C_p T^j}\right], \tag{5}$$

where l^{ij} is the amount of condensed water (if any) produced in displacing the environment from level i to level j.

We require that θ_{lm}^{ij} (the θ_l of the mixture displaced to level j) equal the θ_l of the environment at j, which is θ^j, assuming that the environment contains no condensed water. Solving (2) for the mixing fraction σ^{ij} then gives

$$\sigma^{ij} = \frac{\theta^j - \theta_{lp}^{ij}}{\theta_l^{ij} - \theta_{lp}^{ij}}, \tag{6}$$

with θ_{lp}^{ij} and θ_l^{ij} given by (4) and (5), respectively.

Thus, for each level i, a finite number of mixing fractions, σ^{ij}, can be determined such that subcloud-layer air mixing with a fraction σ^{ij} of environmental air at level i will arrive at level j with a θ_l equal to that of its environment. The maximum number of j's is equal to the maximum number of i's, i.e., INB − ICB. Having determined the σ^{ij}, the updraft mass flux M^i is then partitioned into the various mixtures such that an equal probability mixing distribution is attained. The mass flux of a particular mixture MENT^{ij}, from level i to level j, is then given by

$$\text{MENT}^{ij} = \frac{M^i(|\sigma^{ij+1} - \sigma^{ij}| + |\sigma^{ij} - \sigma^{ij-1}|)}{(1 - \sigma^{ij}) \sum_{j=\text{ICB}-1}^{\text{INB}} [|\sigma^{ij+1} - \sigma^{ij}| + |\sigma^{ij} - \sigma^{ij-1}|]}, \tag{7}$$

provided $0 < \sigma^{ij} < 1$.

Associated with each entrained air flux MENT^{ij} will be a total water content (before precipitation removal) given by

$$\text{QENT}^{ij} = \sigma^{ij} r^i + (1 - \sigma^{ij})(r^i - \epsilon^i l_a^i), \tag{8}$$

where r^i is the environmental mixing ratio at level i.

It should be noted that the fluxes MENT^{ij} are unique functions of the fluxes M^i and the environmental moisture and temperature distributions.

b. Unsaturated downdrafts

At most, only one unsaturated downdraft is assumed to be present at each horizontal grid point at each time step. It is driven by the evaporation of precipitation contributed by updrafts penetrating to each level at which $\epsilon^i > 0$ between cloud base (ICB) and cloud top (INB). These include updrafts of mixed as well as undilute air.

It is further assumed that the unsaturated downdraft adjusts to environmental conditions on a time scale much shorter than that characterizing variations in the large-scale flow. To determine the evaporation rate, it is necessary to determine the precipitation content of the unsaturated downdraft. In this scheme, the precipitation content is found by integrating the conservation equation

$$\frac{d}{dp}(\omega_T l_p \sigma_D)^i = \frac{g}{\Delta p}\epsilon^i l_a{}^i M^i + \frac{g}{\Delta p}\epsilon^i \sum_{j=1}^{i-1}[\mathrm{QENT}^{ji} - r^{*i}]\mathrm{MENT}^{ji} - \sigma_d \sigma_s{}^i E^i, \quad (9)$$

where ω_T is the terminal "omega" of the precipitation, l_p is the precipitation mixing ratio, σ_d is the fractional area covered by the downdraft, Δp is the difference in pressure between two levels centered at i, r^{*i} is the saturation mixing ratio at level i, and E^i is the rate of evaporation of precipitation. The parameter $\sigma_s{}^i$ will be discussed presently.

In deriving (9) I have neglected the vertical advection of precipitation in comparison to its fall velocity and have assumed that the downdraft is steady on the time scale of the large-scale flow. The first and second terms on the right are the rate of detrainment of precipitation from updrafts terminating at level i, and the third term is the loss of precipitation by evaporation. Note that the surface precipitation rate, P, is given by

$$P = (g^{-1}\omega_T l_p \sigma_d)^{i=0}. \quad (10)$$

The terminal "omega," ω_T, and the evaporation rate, E, are in general functions of the precipitation mixing ratio, the environmental thermodynamic properties, and the form of the precipitation (e.g., rain, snow, graupel, etc.). For the present, I assume that all precipitation occurs in the form of rain, though this assumption may be easily relaxed. I consider the forms of ω_T and E used by Klemp and Wilhelmson (1978) and attributed originally to Ogura and Takahashi (1971), i.e.,

$$\omega_T{}^i = 73.45(p^i/T_v{}^i)^{0.6346}(l_p{}^i)^{0.1346}, \quad (11a)$$

$$E^i = \frac{(T_v{}^i/p^i)^{0.475}(1 - r_p^{*i}/r^{*i})C(l_p{}^i)^{0.525}}{1.23 \times 10^4 + 5.83 \times 10^4/(p^i r^{*i})}, \quad (11b)$$

where

$$C = 1.6 + 24.55\left(\frac{p^i l_p{}^i}{T_v{}^i}\right)^{0.2046}, \quad (11c)$$

and r_p^{*i} is a provisional estimate of the mixing ratio of the downdraft, to be discussed presently. In equations (11), p^i is in millibars, T_v in degrees kelvin, and l^i, r_p^{*i}, and r^{*i} in grams per gram, yielding terminal velocities in the units of kg m^{-1} s^{-3} and evaporation rates in s^{-1}. For the purpose of calculating the evaporation of precipitation, we need to estimate the water vapor mixing ratio of the plume. It proves too costly to simultaneously solve (9), (11), (13), and (14) for the plume quantities; instead we estimate $r_p{}^i$ in (11b) by assuming that equivalent potential temperature is nearly conserved in the downdraft over one grid interval in p. The provisional estimate of r_p is the average between this and the environmental r^i. This temporary estimate, $(r_p{}^t)^i$, is used in the evaporation equation. [A more exact estimate is then made by solving (13) and (14).] Moreover, in view of the potential use of this scheme in climate models, where integration time is a serious concern, (11) is replaced by the following approximations:

$$\omega_T{}^i = 0.45 \text{ mb s}^{-1} \quad (12a)$$

$$E^i = \frac{(1 - (r_p{}^t)^i/r^{*i})\sqrt{l_p{}^i}}{2 \times 10^3 + 10^4/(p^i r^{*i})}, \quad (12b)$$

where the mixing ratios are in kg kg^{-1} and pressure is in mb. There was little difference noticed between integrations using (12) and those using (11).

One problem in formulating this scheme is that in nature, some of the precipitation generally falls back through the cloud and thus does not evaporate until it falls through cloud base, while the rest falls into the environment. I have attempted to account for this in a rather crude way by multiplying E^i in (9) by a fraction $\sigma_s{}^i$ (which may be a function of height), where $0 \leqslant \sigma_s{}^i \leqslant 1$. The parameter $\sigma_s{}^i$ is approximately the fraction of precipitation that falls through the environment rather than through the cloud. To always ensure that $\sigma_s{}^i = 1$ for $i <$ ICB, all precipitation is subject to evaporation below cloud base, that is, $\sigma_s{}^i = 1$ for $i <$ ICB.

Once the evaporation rate is found from the precipitation content equation (9) and the evaporation law (12b), the thermodynamic properties and mass flux of the unsaturated downdrafts are found by solving conservation equations for momentum, heat, and water. I consider the downdraft to be a plume with no turbulent entrainment. Neglecting time dependence and nonhydrostatic pressure perturbations, conservation of momentum gives

$$\left(\frac{dM_p{}^2}{dp}\right)^i = -\frac{\rho^i \sigma_d{}^2}{\theta^i}(\theta_p{}^i - \theta^i), \quad (13a)$$

where $M_p{}^i$ is the mass flux of the unsaturated downdraft, defined positive downward, and $\theta_p{}^i$ is the potential temperature of the plume. Effects of water substance on buoyancy have been neglected. Under the same approximations, the thermodynamic equation is written

$$M_p{}^i \frac{g}{\theta^i}\left(\frac{d\theta_p}{dp}\right)^i = -\frac{\sigma_d \sigma_s{}^i L_v E^i}{C_p T^i} + \mathcal{E}_\theta, \quad (13b)$$

where

$$\mathcal{E}_\theta \equiv \begin{cases} \frac{g}{\theta^i}(\theta^i - \theta_p{}^i)\frac{dM_p}{dp}, & \frac{dM_p}{dp} > 0 \\ 0, & \frac{dM_p}{dp} \leqslant 0, \end{cases} \quad (13c)$$

L_v is the latent heat of vaporization, and C_p is the heat capacity of air at constant pressure.

Equations (13a, b, c) are solved simultaneously for $M_p{}^i$ and $\theta_p{}^i$. Conservation of water yields the vapor mixing ratio, r_p, of the downdraft:

$$gM_p{}^i\left(\frac{dr_p}{dp}\right)^i = \sigma_s{}^i \sigma_d E^i + \mathcal{E}_r, \quad (14a)$$

where

$$\mathcal{E}_r \equiv \begin{cases} g(r^i - r_p{}^i)\frac{dM_p}{dp}, & \frac{dM_p}{dp} > 0 \\ 0, & \frac{dM_p}{dp} \leqslant 0. \end{cases} \quad (14b)$$

The terms $\mathcal{E}_\theta$ and $\mathcal{E}_r$ in (13) and (14) represent the "dynamical" entrainment of environmental air into the downdraft.

The solutions of (13) and (14) yield the unsaturated downdraft mass flux as well as the temperature and water vapor content of the downdraft. These in turn yield the fluxes of heat and water by the unsaturated downdraft.

Once again, the time involved in the numerical solution of (13) is a matter of concern. To save time, we first approximate the solution by its hydrostatic equivalent

$$M_p{}^i = \frac{\sigma_d \sigma_s{}^i L_v E^i \theta^i}{C_p g T^i(-d\theta^i/dp)}, \quad (15)$$

and then check a posteriori if the hydrostatic equation is violated. To do so, I check to see if the magnitude of the buoyancy is much smaller than an estimate of the buoyancy made by assuming that θ_p is conserved; i.e., it is required that

$$|\theta_p{}^i - \theta^i| \ll \left|\Delta p \frac{\partial \theta}{\partial p}\right|.$$

Using (13a) and making a reasonable assumption about what is meant by "much smaller than," we impose the condition

$$|(M_p{}^{i+1})^2 - (M_p{}^i)^2| < 0.1\rho^i \sigma_d{}^2 \frac{\theta^i - \theta^{i-1}}{\theta^i}\Delta p. \quad (16)$$

If (16) is violated, then Eqs. (13a–c) are solved simultaneously.

c. Determination of the undilute updraft mass fluxes, M^i

With the specification of the precipitation efficiencies, ϵ^i, the fraction of precipitation falling through the unsaturated environment, $\sigma_s{}^i$, and the fractional area covered by precipitating downdrafts, σ_d, the tendencies of temperature and water vapor depend only on the fluxes M^i of undilute boundary-layer air to level i. It is important to note that, if the environmental forcing of convection (e.g., surface fluxes and radiative cooling) is known, the M^i must be such that the convective tendencies balance the large-scale tendencies over a sufficient length of time, as pointed out by Arakawa and Schubert (1974). The M^i are not actually forced to meet this condition, but are adjusted with time towards quasi-equilibrium.

One may regard a convective flux averaged over a large-scale grid box as the product of a fractional area, σ^i, and a vertical velocity, w^i. Thus $M^i = \sigma^i \rho^i w^i$, where ρ^i is the air density at level i. The vertical velocity is estimated from the subcloud parcel's convective available potential energy (CAPE):

$$w^i = \sqrt{2\text{CAPE}^i}, \quad (17a)$$

where

$$\text{CAPE}^i = \sum_{n=\text{ICB}}^{i} R_d(T_{vp}^n - T_v{}^n)\Delta \ln p. \quad (17b)$$

Suppose for the time being that the σ^i are fixed constants. Then the control of the mass fluxes M^i in any large-scale model employing this scheme can be through any or all of the following:

(i) large-scale control of CAPE^i,

(ii) control of the temporal frequency of the occurrence of M^i by regulating the altitude INB or by switching on and off the condition for convection, or

(iii) control of the fraction of grid points experiencing convection within a small area at a given time.

In a one-dimensional radiative–convective equilibrium model, for example, controls (i) and (ii) may operate. In this case, experiments using this scheme with fixed σ^i lead to the following conclusions:

1) If σ^i is relatively large, the convective tendencies at a particular time step are large and the model atmosphere overstabilizes, leading to no convection for one or several subsequent time steps. The control of M^i is largely through process (ii) above. The *time-average* value of CAPE^i may be negative.

2) If σ^i is relatively small, convection cannot balance forcing unless CAPE^i is large. The control of M^i is then exclusively through process *a* above and the time-average CAPE^i is positive.

Perhaps not surprisingly, the time-averaged M^i are very nearly identical in cases 1 and 2, and the vertical profiles of relative humidity are also very similar. The only difference is in the vertical profile of temperature,

which may depart ±1° or 2°C from moist adiabatic in each case, and in the "noisiness" of the simulation. One can argue convincingly that the determination of the σ^i's is a secondary issue for quasi-equilibrium convection; they become more of an issue for "stored-energy" convection of the kind experienced over continents under some conditions.

In spite of the preceding observation, it would be nice to predict or diagnose the fractional areas σ^i covered by updrafts. To do so, I again consider a case in which the large-scale production of buoyancy for subcloud air is known. Suppose one has a neutral sounding at the beginning of a time step, Δt. At the end of the time step the large-scale forcing produces a positive buoyancy profile for lifted subcloud air. Starting with a fixed but very small σ^i I calculate the convective tendency of buoyancy and add it to the first profile, producing the second, slightly less unstable, profile. Imagine repeating this "convective step" many times until there is no buoyancy at the *lowest* grid point, at which point convection will turn off *even* if there is still buoyancy above this point (i.e., the sounding is *conditionally* unstable). This presents a dilemma, illustrated by two extreme scenarios.

Suppose on the one hand that convection acts in such a way as to first eradicate the buoyancy at the uppermost grid point for which the buoyancy was initially positive. Convection then continues until the next grid point down is stabilized, with the stabilization proceeding downward until the lowest grid point is stabilized. The resulting sounding will be stable or neutral.

On the other hand, it may be that the activity of shallow drafts produces neutrality at the lowest grid point before the deeper drafts have stabilized the upper part of the sounding; the convection then turns off, leaving a conditionally unstable sounding.

It is not a priori clear which of these two extremes to favor. We proceed by assuming that the instantaneous convective tendencies of CAPE act in a *direction* so as to drive the individual mass fluxes, M^i, toward quasi-equilibrium with the large-scale forcing.

Suppose we calculate w^i from the sounding at a particular grid point at two different times. With fixed σ^i, the change in mass flux M^i between the two time steps will be

$$\delta M^i = \rho^i \sigma^i \delta w^i. \tag{18}$$

In order to drive the system more rapidly toward quasi-equilibrium, we increase or decrease the fractional area σ^i so as to produce the same effect as a change in the CAPE^i:

$$\delta \sigma^i = \alpha^i \delta w^i, \tag{19}$$

where α^i is a multiplier that may depend on pressure. By applying (19) the system is driven toward quasi-equilibrium by changes in the fractional coverage of drafts as well as by changes in CAPE^i. If α^i is large, one can achieve large changes in the mass flux without appreciable changes in the sounding's CAPE^i. I choose α^i to give relatively smooth evolution of the mass flux; tests show that the equilibrium profiles are insensitive to α^i within a reasonable range.

When (19) is applied, it is possible for the system to reach equilibrium at large values of w^i and small values of σ^i, implying a reservoir of energy that could be used for more convection. (This tends to happen only when the large-scale forcing is steady over periods of many days.) To prevent this, we add a small constant tendency to σ^i that is reversed when convection ceases at a particular grid point and level:

$$\delta \sigma^i = \begin{cases} \alpha^i \delta w^i + \beta, & w^i > 0 \\ \alpha^i \delta w^i - \beta, & w^i = 0, \end{cases} \tag{20}$$

with β very small.

In summary, the mass fluxes are calculated according to

$$M^i = \rho^i \sigma^i w^i,$$

with w^i given by (17) and σ^i adjusted according to (20). At the initial time, and if there has been no convection for ten time steps, the σ^i are set to zero.

d. Heating and moistening by convection

The convective forcing of potential temperature results from condensation, evaporation, and fluxes of heat by updrafts and downdrafts.

Confining our attention first to in-cloud drafts, the tendency of potential temperature may be written

$$\left(\frac{\partial \theta}{\partial t}\right)_{sd} = \frac{g}{\theta}\frac{\partial}{\partial p}(M(\theta_c - \theta)) - gM\frac{\partial \theta_c}{\partial p} - \frac{L_v \theta}{C_p T} E_d, \tag{21}$$

where M is the *net* upward mass flux at level i, θ_c is the potential temperature of the cloud, and E_d is a term representing the evaporation of detrained condensate. The first term on the right of (21) is the eddy flux of potential temperature while the second is the heating due to the condensation. Due to cancellation among some of the terms, (21) may be written in the alternative form

$$\left(\frac{\partial \theta}{\partial t}\right)_{sd} = -gM\frac{\partial \theta}{\partial p} - \left\{\frac{L_v \theta}{C_p T} E_d - \frac{g}{\theta}(\theta_c - \theta)\frac{\partial M}{\partial p}\right\}. \tag{22}$$

In this form, the warming can be interpreted as due to forced subsidence in the environment (first term on the right), evaporation of detrained condensate, and detrainment of cloudy air with a temperature different from the environment.

The term in brackets in (22) is handled by assuming that liquid water potential temperature is conserved as condensate reevaporates on detrainment. Recall that we have calculated the detrainment levels of mixed

parcels by insisting that the liquid water potential temperature of the detrained air equal that of its environment. Thus, for these drafts the term in brackets in (22) vanishes. The one exception to this rule is if there are *no* detrainment levels for air entraining at a particular level i; this will sometimes be true at the level of cloud top, INB, for example. In that case, the term in brackets in (22) becomes

$$-\frac{L_v\theta}{C_pT}E_d+\frac{g}{\theta}(\theta_c-\theta)\frac{\partial M}{\partial p}=\frac{g}{\theta^i}(\theta^i_{lc}-\theta^i)\frac{M^i}{\Delta p}\delta^i, \tag{23}$$

where θ^i_{lc} is the liquid water potential temperature of the subcloud air lifted to level i *after* it has been depleted of precipitation, and

$$\delta^i\equiv\begin{cases}1, & \text{if } N^i=0\\ 0, & \text{otherwise,}\end{cases} \tag{24}$$

where N^i is the number of drafts entraining at level i.

The *net* mass flux at any level i is given by

$$M=\sum_{n=i}^{\mathrm{INB}}M^i+\sum_{n=1}^{i-1}\sum_{k=i}^{\mathrm{INB}}\mathrm{MENT}^{n,k}-\sum_{n=i}^{\mathrm{INB}}\sum_{k=1}^{i-1}\mathrm{MENT}^{n,k}, \tag{25}$$

with $\mathrm{MENT}^{n,k}$ given by (7). The first term on the right of (25) is the contribution from all updrafts penetrating to a level i or higher, while the second term represents the upward mass flux in all buoyancy-sorting drafts originating at level i or higher and detraining at level $i-1$ or lower. The last term in (25) likewise represents the downward flux by all buoyancy-sorting drafts entraining at level i or higher and detraining at level $i-1$ or lower.

The tendency of potential temperature due to unsaturated downdrafts is

$$\left(\frac{\partial\theta}{\partial t}\right)_{ud}=-\frac{g}{\theta}\frac{\partial}{\partial p}(M_p(\theta_p-\theta))-\theta\frac{L_v}{C_pT}\sigma_d\sigma_sE, \tag{26}$$

where M_p is the net *downward* mass flux in the unsaturated downdraft and E is the evaporation rate.

Using the above together with (22), (23), and (25), the total convective tendency of potential temperature is

$$\left(\frac{\partial\theta}{\partial t}\right)^i=-g\left(\frac{\partial\theta}{\partial p}\right)^i\sum_{n=i}^{\mathrm{INB}}(M^n+\sum_{k=1}^{i-1}(\mathrm{MENT}^{k,n}-\mathrm{MENT}^{n,k}))+\frac{g}{\theta^i}(\theta^i_{lc}-\theta^i)\frac{M^i}{\Delta p}\delta^i-\frac{g}{\theta^i}\frac{\partial}{\partial p}[M_p{}^i(\theta_p{}^i-\theta^i)]-\theta^i\frac{L_v}{C_pT^i}\sigma_d\sigma_s{}^iE^i, \tag{27}$$

with δ^i given by (24), $M_p{}^i$ and $\theta_p{}^i$ obtained by solving (13) [or (15) with $\theta_p{}^i=\theta^i$, if (16) is satisfied], and E^i given by (12b).

By analogy with the preceding development, the water vapor mixing ratio tendency due to in-cloud updrafts and downdrafts is given by

$$\left(\frac{\partial r}{\partial t}\right)_{sd}=g\frac{\partial}{\partial p}[M(Q_c-r)]-gM\frac{\partial Q_c}{\partial p}=-gM\frac{\partial r}{\partial p}+g(Q_c-r)\frac{\partial M}{\partial p}, \tag{28}$$

with M given by (25) and Q_c is the total water mixing ratio in the undilute updraft or in the buoyancy-sorting draft, after the precipitation has been removed. According to (28), the large-scale water vapor field is affected by advection of environmental water vapor by compensating updrafts and downdrafts outside the clouds and by detrainment of water substance.

Accounting for the various updrafts and downdrafts and for evaporation of precipitation, (28) may be written

$$\left(\frac{\partial r}{\partial t}\right)^i=-g\left(\frac{\partial r}{\partial p}\right)^i\sum_{n=i}^{\mathrm{INB}}(M^n+\sum_{k=1}^{i-1}(\mathrm{MENT}^{k,n}-\mathrm{MENT}^{n,k}))+\frac{g}{\Delta p}\sum_{n=1}^{\mathrm{INB}}\mathrm{MENT}^{n,i}(\mathrm{QENT}^{n,i}-\epsilon^i l^{n,i}-r^i)+\frac{g}{\Delta p}M^i\delta^i(r^1-\epsilon^i l_a{}^i-r^i)-g\frac{\partial}{\partial p}[M_p{}^i(r_p{}^i-r^i)]+\sigma_d\sigma_s{}^iE^i. \tag{29}$$

Here $l^{n,i}$ is the adiabatic condensed water content of the buoyancy-sorting draft.

The water vapor content is affected by (i) vertical advection of environmental water vapor by compensating updrafts and downdrafts, (ii) detrainment of water substance (including condensate) at the termination of in-cloud drafts, (iii) downward advection of dry air by unsaturated downdrafts, and (iv) evaporation of falling precipitation.

The total representation of heating and moistening is given by (27) and (29), with the in-cloud draft fluxes given by (4)–(7), (17), (19), and (20), and the evaporation given by (12b). [In order to find E^i, it is necessary to first determine the precipitation content from (9).] The switch δ^i is given by (24).

The parameters that must be specified (or diagnosed) in this scheme are the parcel precipitation efficiencies, ϵ^i, the fraction of precipitation, $\sigma_s{}^i$, that falls outside of

clouds, and the fractional area covered by precipitating downdrafts. I shall return in section 4 to a discussion of these parameters.

e. Subroutine CONVECT

The scheme described herein has been coded in the form of a standard FORTRAN 77 subroutine. One must provide one-dimensional (vertical) arrays of temperature, mixing ratio, and pressure. The subroutine returns the convectively produced local time tendencies of potential temperature and water vapor mixing ratio, together with the convective precipitation rate.

The tendency equations (27) and (29) are solved in finite-difference form using upstream differencing in the advection terms for stability. The scheme exactly conserves water substance so that the finite difference sum of the water-vapor tendencies exactly equals the precipitation. It has been successfully run in ten-day integrations of the T106 version of the European Centre for Medium Range Weather Forecasts global forecast model.

This subroutine is available from the author for the cost of reproduction and mailing.

4. One-dimensional equilibrium calculations

a. Specification of ϵ^i, σ_d, and $\sigma_s{}^i$

The character of the profiles of heating and moistening produced by the scheme are dependent on the parcel precipitation efficiencies, ϵ^i, the fractional area covered by the precipitating downdraft, σ_d, and the fraction of precipitation that falls through unsaturated environment, $\sigma_s{}^i$.

The fraction of condensed water, ϵ^i, converted to precipitation in an individual updraft ascending to level i is in nature a function of the total amount of condensate produced, the air temperature up to and including the level i, the type and size distribution of condensation and freezing nuclei, the actual updraft velocity, and the amount and type of precipitation falling through the updraft. Qualitatively, one may expect that ϵ^i increases from zero near cloud base to close to unity in the upper troposphere. Trade cumuli have ϵ^i close to zero, for example. For the present purpose of showing the general nature of the scheme, we specify ϵ^i according to:

$$\epsilon^i = \begin{cases} 0, & p^{\mathrm{ICB}} - p^i < p^c \\ \dfrac{p^{\mathrm{ICB}} - p^i - p^c}{p^t - p^c}, & p^c < p^{\mathrm{ICB}} - p^i < p^t \\ 1, & p^{\mathrm{ICB}} - p^i > p^t, \end{cases} \quad (30)$$

where p^c is a critical cloud depth (in pressure), here taken to be 150 mb, below which no precipitation is permitted to form and p^t is a critical cloud depth (in pressure) above which all condensate is converted to precipitation. The precipitation efficiency varies linearly between these two limits. I take $p^t = 500$ mb.

The present, provisional, specification of ϵ^i as a function of pressure and ICB is not an inherent limitation of the scheme, since ϵ^i could be determined as a function of other model variables such as water content and temperature.

Specification of $\sigma_s{}^i$ is more problematic, since the amount of precipitation falling back through clouds, as opposed to falling through clear air, is highly dependent on the exact configuration of the cloud, its slope, presence of anvil, etc. Houze (1982) and others note that a significant amount of tropical precipitation associated with convective systems falls from the mesoscale anvil shield. Once again, I specify a profile of $\sigma_s{}^i$ for the sake of expedience, avoiding for the time being a more involved approach to the problem, by setting it equal to 0.15 at and above cloud base and 1.0 below cloud base.

Were it not for the square root dependence of evaporation on condensed water mixing ratio, (12b), the parameter σ_d would only appear in the product $\sigma_d l_p{}^i$ and would thus not be a real parameter; that is, it would not be necessary to predict σ_d and $l_p{}^i$ separately. If (9) and (12b) are rephrased in terms of $\sigma_d l_p{}^i$, it becomes apparent that the evaporation rate depends on $\sqrt{\sigma_d}$. Thus, the real dependence on σ_d is rather weak. I choose a specification of σ_d that yields reasonable values of the precipitation content $l_p{}^i$. The value used in the present scheme is

$$\sigma_d = 0.01. \quad (31)$$

The total number of adjustable parameters is $2N + 1$, where N is the number of model levels between cloud base and cloud top. It may be legitimately complained that this is such a large set that any result desired may be achieved. This is, of course, true within limits. But the parameters ϵ^i, σ_d, and $\sigma_s{}^i$ represent just those cloud physical properties that one arguably needs to know to represent in a realistic way the effects of ensembles of subcloud-scale updrafts and downdrafts. They represent the physical processes responsible for determining how much condensed water reevaporates, thus moistening and cooling the air, and how much falls out of the system, leading to warming and drying. This distinction is critical for everything from the dynamics of mesoscale systems to climate, and its roots in cloud microphysics cannot be disregarded. I have attempted here to link as closely as is feasible the important parameters of the present convective scheme to cloud microphysics, though one could hope to do better.

Ideally, one could estimate ϵ^i, σ_d, and $\sigma_s{}^i$ within certain limits from theory and observations. They could then be tuned within these limits by running the scheme in "semiprognostic" mode using experimental datasets such as those from GATE, optimizing the agreement between fields produced by the scheme and observa-

tions. The ability of the scheme to predict the evolution of the large-scale relative humidity field given only the large-scale vertical velocity, radiation, surface fluxes, and horizontal advection should be a particularly sensitive test of the scheme. For the time being, however, I will specify provisional estimates of the parameters as discussed previously.

The rate of approach of the mass fluxes to quasi-equilibrium is controlled by the parameter α^i. A smooth evolution of the mass fluxes is provided by taking

$$\alpha^i = 0.004/(p^{\mathrm{ICB}} - p^i),$$
$$\beta = 5 \times 10^{-8},$$

with p given in mb.

b. A simple radiative-convective equilibrium calculation over the tropical ocean

As a straightforward test of the new scheme, a radiative-moist convective equilibrium calculation is performed. In this calculation the entire atmosphere from 150 mb down to the surface is cooled at the constant rate of 3×10^{-5} K s^{-1} (2.6°C day^{-1}). This cooling is compensated for by fluxes of sensible and latent heat from the ocean, calculated according to bulk aerodynamic formulae:

$$F_\theta = C_D|V|(\theta^s - \theta^1) \tag{32a}$$

$$F_r = C_D|V|(r^{*s} - r^1), \tag{32b}$$

where C_D is a dimensionless exchange coefficient, here taken to be 2×10^{-3}, $|V|$ is a mean surface wind, θ^s is the potential temperature of the sea surface, and r^{*s} is the saturation mixing ratio at sea surface temperature and pressure; θ^1 and r^1 are the model-determined values of θ and r at the lowest grid point. For the present calculation, $|V| = 5$ m s^{-1} and $\theta^s = 300$ K at a pressure of 1025 mb.

The model is initialized, somewhat arbitrarily, using a particular sounding from the tropical western Pacific. It is run at 20-min time steps to 800 hours. The vertical grid pressure interval is 50 mb up to 200 mb, then 25 mb up to 100 mb.

The time evolutions of the precipitation, evaporation, lowest level potential temperature, and mixing ratio are shown in Figs. 3a–c for the entire integration period. These variables have been smoothed by a 36-h running mean.

The fields approach equilibrium over a period of several hundred hours. This time scale reflects the amount of time needed for an individual parcel to complete one full circuit of saturated ascent followed by unsaturated descent under the influence of radiative cooling; this is about 300 h in the present case. While the convective mass fluxes come into equilibrium with the large-scale forcing very rapidly, the equilibrium water vapor is established over many tens of days due to the long residence time of water outside of clouds.

The entropy sources and sinks, averaged over the last 5 days of the simulation, are shown in Fig. 3d. The net convective heating balances the radiative cooling, except in the boundary layer, where surface sensible heat fluxes are important, and in a thin layer near the tropopause, where slight overshooting (since INB is *above* the level of neutral buoyancy) produces an uncompensated cooling. Convection is actually cooling the boundary layer by rain evaporation.

The contributions of convective and surface fluxes to the water balance are shown in Fig. 3e, which also represents an average over the final 5 days of the simulation. In the interior, the detrainment of water by convective drafts and moistening by evaporation or precipitation balance the drying by subsidence in the environment. Near the surface, drying by downdrafts balances surface evaporation.

The total vertical mass fluxes by in-cloud updrafts and downdrafts, and by unsaturated downdrafts, averaged over the last 5 days, are shown in Fig. 3f. The fluxes by in-cloud updrafts (solid line in Fig. 3f) peak at cloud base, and in spite of entrainment, decrease with height except near the tropopause. Fluxes by cloudy downdrafts peak at 800 mb and are negligible above 500 mb. The precipitation-driven downdraft mass flux peaks in the boundary layer since evaporation of precipitation is greatest there while the static stability is small or zero.

The mass flux profiles in Fig. 3f are not unlike those derived from observations of tropical mesoscale systems (Houze 1988; Johnson 1984). The *net* mass flux in the steady state is completely dictated by the specified radiative cooling since the latter must be exactly balanced by the net convective heating. But the partitioning of the mass fluxes between updrafts, saturated downdrafts, and unsaturated downdrafts does depend on the details of the scheme.

The entrainment and detrainment of mass into and from in-cloud drafts is shown in Fig. 3g. Entrainment into cloud base produces a large maximum in the subcloud layer. The entrainment maximum near 750 mb is associated with penetrative downdrafts, while the one near 200 mb represents entrainment into updrafts. Detrainment from updrafts is large above 500 mb and shows a sharp peak at the tropopause. The detrainment below 600 mb mostly represents detrainment from penetrative downdrafts. Entrainment into and detrainment from the precipitating downdraft may be deduced from the mass flux profile in Fig. 3f.

The fractional areas (σ^i) covered by undilute updrafts (M^i), averaged over the last 5 days of the integrations, are shown in Fig. 3h. (These should not be interpreted as fractional areas of clouds themselves, since the latter reflect not only the undiluted parcels, which constitute a relatively small fraction of cloudy air, but also active buoyancy-sorting drafts and "debris" of decaying, nearly neutrally buoyant air.) The spectrum is somewhat bimodal, with a sharp peak representing shallow drafts, or clouds, around 900 mb.

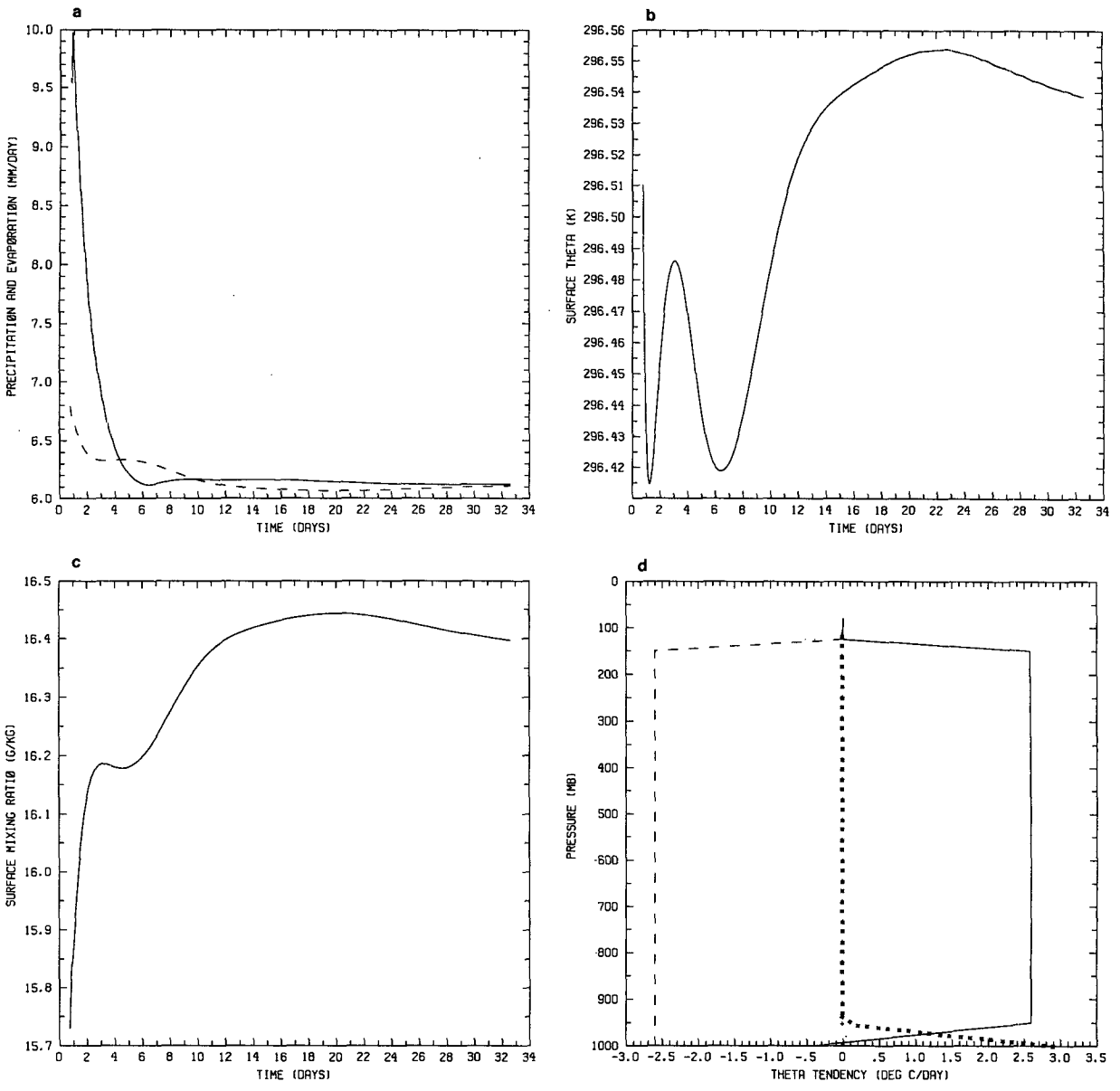

FIG. 3. Results of the radiative–convective equilibrium calculations: (a) evolution with time (hours) of the convective precipitation (solid) and surface evaporation (dashed), in mm day^{-1}. Values smoothed with 36-h running mean. (b) As in (a) except for lowest model level potential temperature (K). (c) As in (a) except for lowest model level mixing ratio (g kg^{-1}). (d) Tendencies of potential temperature (K day^{-1}) due to various processes, averaged over the last 100 hours of model run. Solid line: all convective processes. Dashed line: radiative cooling. Dotted line: surface fluxes.

The thermodynamic characteristics of the equilibrium state are portrayed in Figs. 3i–l, which again represent quantities averaged over the last 5 days of integration. Figure 3i shows the average buoyancy of a lifted subcloud-layer parcel. In spite of the adjustment of the mass fluxes toward quasi-equilibrium, significant amounts of buoyancy remain in the lower and in the upper troposphere. The reason for the upper-tropospheric buoyancy is as follows: The constant radiative cooling demands a net mass flux that increases with height in the upper troposphere, since $M \approx \dot{Q}/(\partial\theta/\partial p)$ and the static stability decreases with height. Mass flux can increase with height only if (i) the downdraft mass flux decreases with height, or (ii) there is entrainment into updrafts. Downdrafts are weak in the upper troposphere as very little evaporation can occur. Thus the only way mass flux can increase with height in the upper troposphere is by entrainment, which *requires* finite buoyancy. The amount of buoyancy evident in the upper troposphere in Fig. 3i is that necessary to maintain the *entrained air* mass flux that is necessary in this case to help balance radiative cooling. The

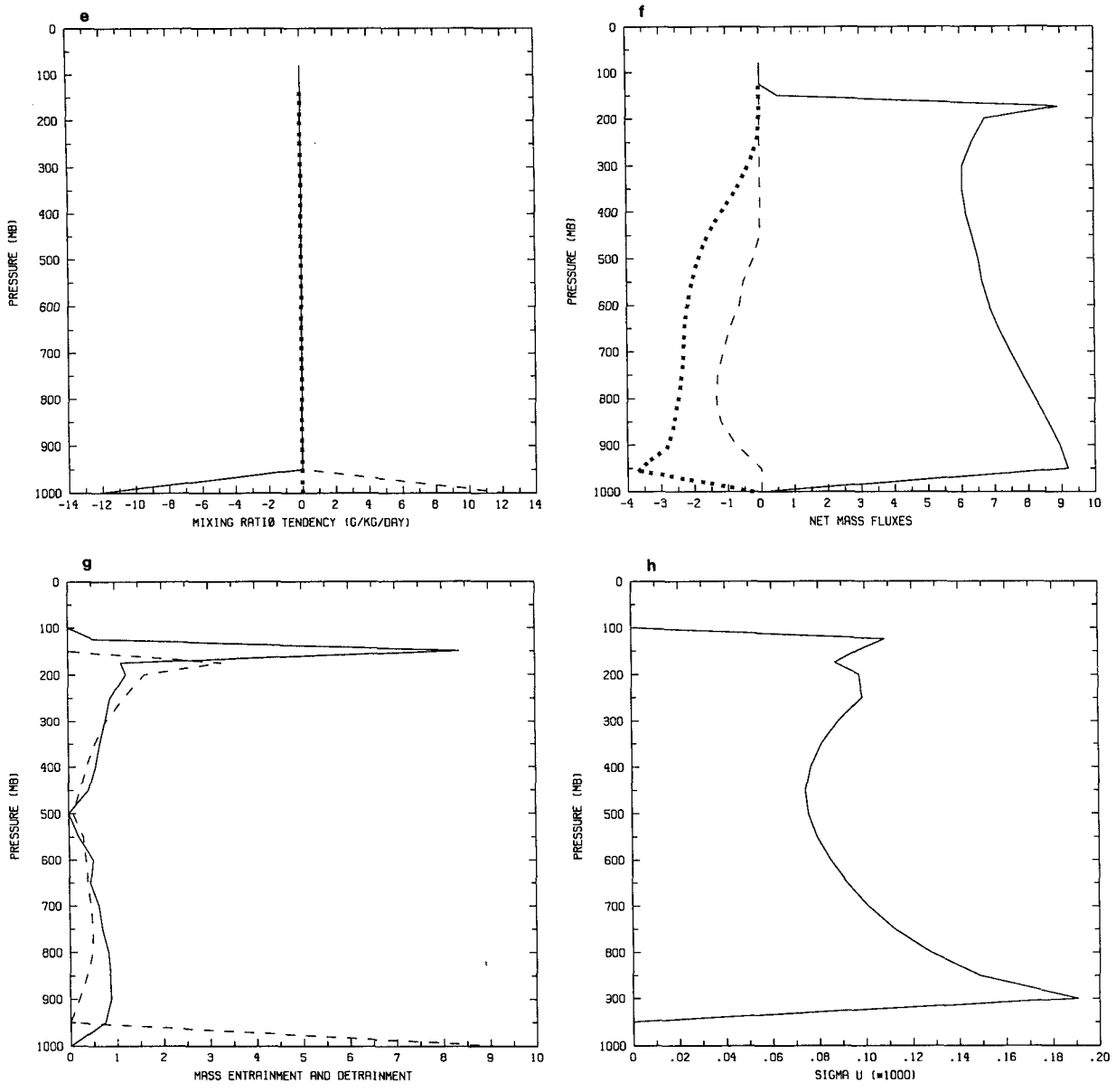

FIG. 3. (*Continued*) (e) Tendencies of mixing ratio (g kg^{-1} day^{-1}) due to various processes, averaged over the last 100 hours of model run. Solid line: all convective processes. Dashed line: surface fluxes. (f) Net mass fluxes (10^{-3} kg m^{-2} s^{-1}) through each pressure level due to various convective drafts, averaged over the last 100 hours of simulation. Solid line: All updraft mass fluxes, including entrained air flux. Dashed line: penetrative downdraft mass flux. Dotted line: mass flux in unsaturated downdraft. (g) Mass detrainment (solid) and entrainment (dashed), in units of 10^{-3} kg m^{-2} s^{-1}, due to in-cloud updrafts and downdrafts at each pressure level. (h) Fractional areas, σ^i, (10^{-3}) covered by undilute updrafts carrying mass flux M^i.

buoyancy profile thus depends on the nature of the large-scale forcing. The lower tropospheric buoyancy maximum is a consequence of the "mixing line" structure established by shallow clouds.

The relative humidity profile is shown in Fig. 3j. The humidity at 1000 mb is not that at sea level, which is at the half-pressure level of 1025 mb; this would be close to 85%. The somewhat unrealistically sharp decrease of relative humidity in the lower troposphere is related to the unrealistically deep layer of imposed radiative cooling. This decrease is reflected in the profile of equivalent potential temperature (θ_e) shown in Fig. 3k; this profile shows a sharp decline in θ_e in the lower troposphere. When plotted on a θ_e–Q diagram (Fig. 3l), the first four points in the sounding fall along a "mixing line" (Betts and Albrecht 1987).

The precipitation mixing ratio and the difference between the vapor mixing ratio of the precipitation-driven downdraft and that of the environment are shown in Fig. 3m. The precipitation content is sensitive to σ_d, varying almost inversely with it, though as mentioned previously the evaporation rate varies more

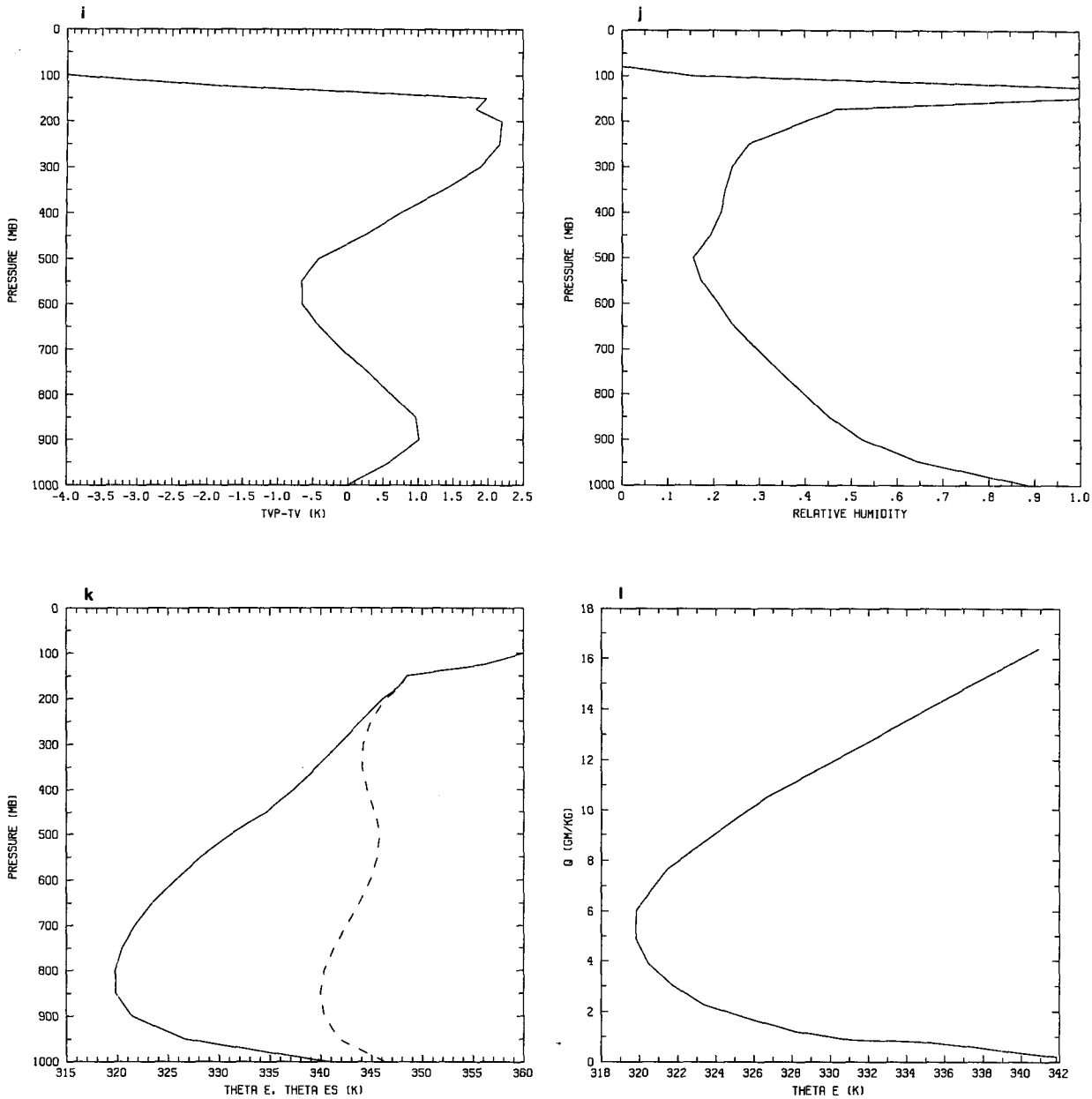

FIG. 3. (*Continued*) (i) The difference between virtual temperature (including condensate loading) of lifted subcloud-layer air and environmental virtual temperature, averaged over the last 100 hours of the simulation. Units in Kelvin. (j) As in (i) but for relative humidity. (k) As in (i) but for equivalent potential temperature (solid) and saturation equivalent potential temperature (dashed). (l) Environmental mixing diagram showing total water (Q) against θ_e (K). (m) As in (h) but for rainwater content (solid) and unsaturated downdraft mixing ratio surplus (dashed), both in g kg^{-1}.

slowly with σ_d. The mixing ratio of the downdraft can be understood by noting that the plume is nearly hydrostatic, so that its temperature is nearly that of its environment. As the plume descends, it takes with it the high-θ_e air of the upper troposphere; this must be reflected by a surplus of mixing ratio since the temperature deficit is negligible. As the plume descends below the level of minimum θ_e, it entrains the low θ_e air from the environment and by the time it reaches the subcloud layer it exhibits a θ_e deficit.

c. *Experiments with fixed fractional areas, σ^i*

Experiments with fixed σ^i show that for sufficiently small values, the convection becomes steady. Reducing it further, however, leads to substantial changes in the equilibrium temperature and water vapor distributions as the atmosphere attempts to compensate for insufficient mass flux by increasing the amount of instability. Figure 4a shows the evolution of precipitation in an experiment in which σ^i is fixed at a small value, dem-

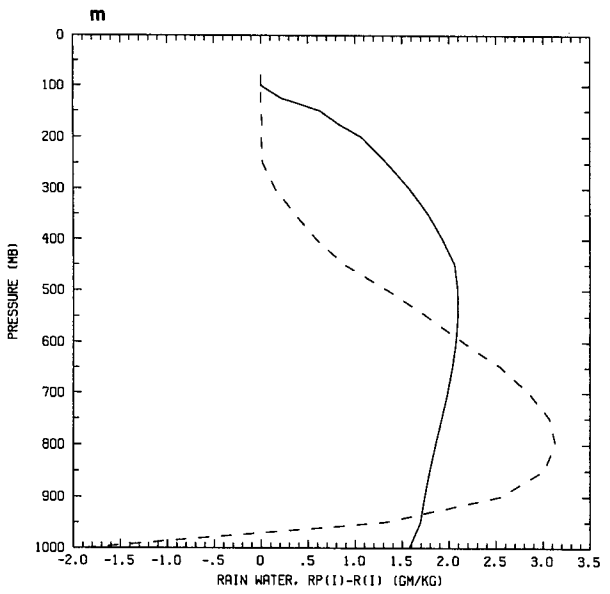

FIG. 3. (*continued*)

onstrating that the system reaches a nearly steady state. The buoyancy profile (Fig. 4b) demonstrates that there is positive buoyancy all the way to the tropopause. In this experiment the mass fluxes are regulated *entirely* by the amount of conditional instability in the sounding, and not by fractional areas or by intermittency. This is unphysical because the existing instability would give rise to more clouds.

At the opposite extreme, we have run an experiment in which σ^i is increased by a factor of ten over the value used to construct Fig. 4. In this experiment the precipitation becomes far more episodic (Fig. 5a). But the resulting time-averaged mass fluxes are very similar to those of the control experiment, illustrating that the environmental forcing and not the specified fractional coverages σ^i is determining the cloud mass fluxes. If the fractional areal coverage is increased, the convection becomes less frequent in time: there is a nearly exact compensation between the density of convection in space and in time. But there are noticeable differences between the relative humidity in this experiment (Fig. 5b) and that of the control (Fig. 3j). The reason for this is interesting and is due to differences in the evaporation of rain. Because the radiative heating is fixed at the same value in each experiment, the time-averaged rainwater reaching the surface must be nearly identical (neglecting small differences in the surface sensible heat flux). In the experiment with episodic convection, this is achieved by intense bursts of heavy rain while in the control the rainfall is steady. But the evaporation varies as the square root of the rainwater, so on average it is less in the episodic case (for the same reason that evaporation varies as $\sqrt{\sigma_d}$, the fractional areal coverage). Thus, the relative humidity at lower levels is less in the episodic case.

If one neglects this effect on the rain evaporation, the calculation of fractional areas σ^i is unnecessary except insofar as it makes the integration a bit smoother. One could simply specify σ^i and, as shown by experiment, as long as it is *overspecified* the model will simply adjust the temporal frequency of convection to yield the required mass flux, although not without effect on the relative humidity field. A three-dimensional model may also take advantage of the extra degrees of freedom in the spatial coverage of convection.

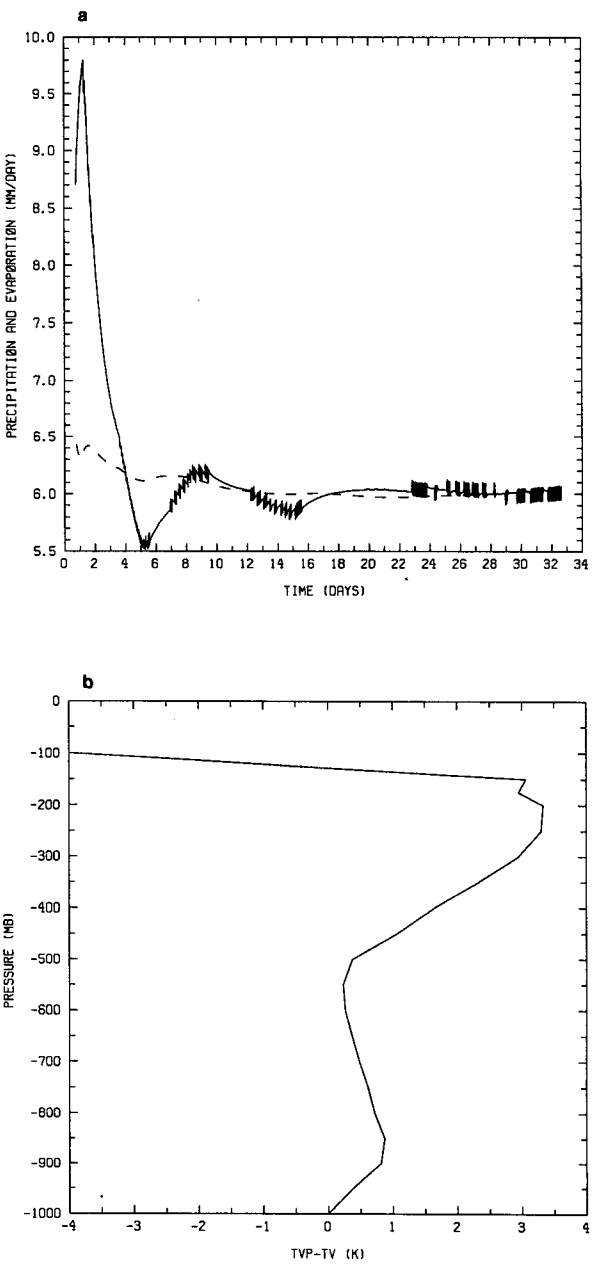

FIG. 4. (a) As in Fig. 3a, but for σ^i fixed at a value of 10^{-4}. (b) Buoyancy, as in Fig. 3i, but for σ^i fixed at 10^{-4}.

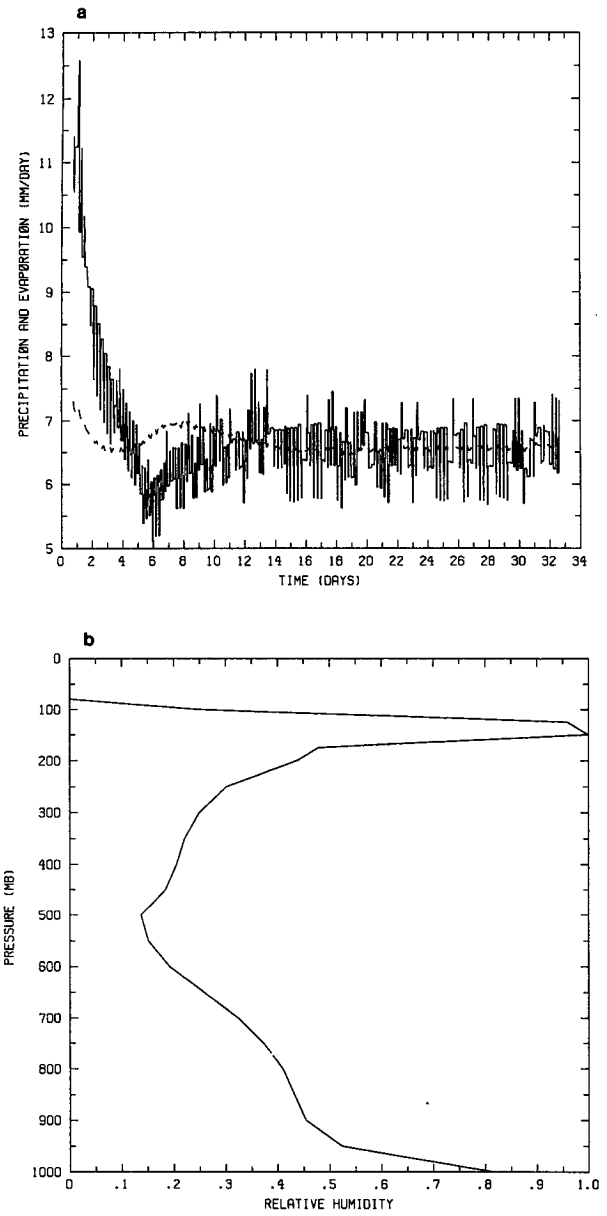

FIG. 5. (a) Same as Fig. 4a but for σ^i fixed at a value of 10^{-3}. (b) Same as (a) but showing relative humidity.

d. *Sensitivity to model parameters*

As one would expect, the model is sensitive to the specification of ϵ^i and $\sigma_s{}^i$. To demonstrate this we have performed two experiments. In the first, all of the condensed water is converted to rain ($\epsilon^i = 1$ for all i) and all of it falls through the cloud ($\sigma_s{}^i = 0$) so that evaporation occurs only below cloud base. The relative humidity profile in this experiment is shown in Fig. 6a. Since no condensate is detrained into the environment, the latter becomes quite dry, particularly in the lower troposphere. It is important to note, however, that water vapor is still detrained from updrafts; this keeps the relative humidity high in the upper troposphere. In particular, the air near the tropopause is still saturated because detrainment is not compensated for by subsidence there.

In this experiment the moistening of the atmosphere is determined entirely by the environmental requirement for convective mass flux. Even with all condensed water removed from the system without reevaporation, convection still moistens the upper troposphere.

The second experiment has a constant parcel precipitation efficiency $\epsilon^i = 0.5$ with $\sigma_s{}^i = 0.15$. This results in excessive detrainment of condensed water at upper levels. As shown in Fig. 6b, the resulting equilibrium relative humidity profile exhibits saturation through the upper troposphere.

If the fraction $\sigma_s{}^i$ of precipitation falling through unsaturated air is increased from 0.15 to 0.3, the main effect is to moisten the lower troposphere by evaporation, as shown in Fig. 6c. The unsaturated downdraft mass fluxes (not shown) are unrealistically large, however.

e. *The effect of large-scale ascent*

The effects of an imposed large-scale upward velocity field have been examined by introducing a pressure velocity

$$\omega = 4\omega_m\left(\frac{(p_0 - p)(p - p_1)}{(p_0 - p_1)^2}\right), \qquad (33)$$

where ω_m is the maximum pressure velocity in the layer, occurring at a pressure $\frac{1}{2}(p_0 + p_1)$, and p_0 and p_1 are the pressure levels at which ω vanishes. In the experiment reported here we take $\omega_m = -30$ mb day^{-1}, $p_0 = 1000$ mb, and $p_1 = 150$ mb. This large-scale ascent advects potential temperature and water vapor mixing ratio.

The results are shown by Fig. 7. The convective heating (Fig. 7a) now peaks in the middle troposphere so as to counter the adiabatic cooling that is maximized there. A net drying of the troposphere by convection (Fig. 7b) also counters the moistening by the large-scale flow. The buoyancy of subcloud-layer air (Fig. 7c) again shows two peaks: one in the lower troposphere and the other just below the tropopause. The overall average CAPE is *less* in this case than in the experiment without imposed upward motion. The tropospheric humidity (Fig. 7d) is larger, as expected.

f. *The effect of large-scale descent*

The results of imposing a large-scale descent, using (33) with $\omega_m = 30$ mb day^{-1}, $p_0 = 1000$ mb, and $p_1 = 200$ mb, are displayed in Fig. 8. Averaged over the last 5 days, the thermodynamic profiles (Fig. 8a) show a strong trade inversion at about 700 mb, above which the relative humidity nearly vanishes (Fig. 8b), because

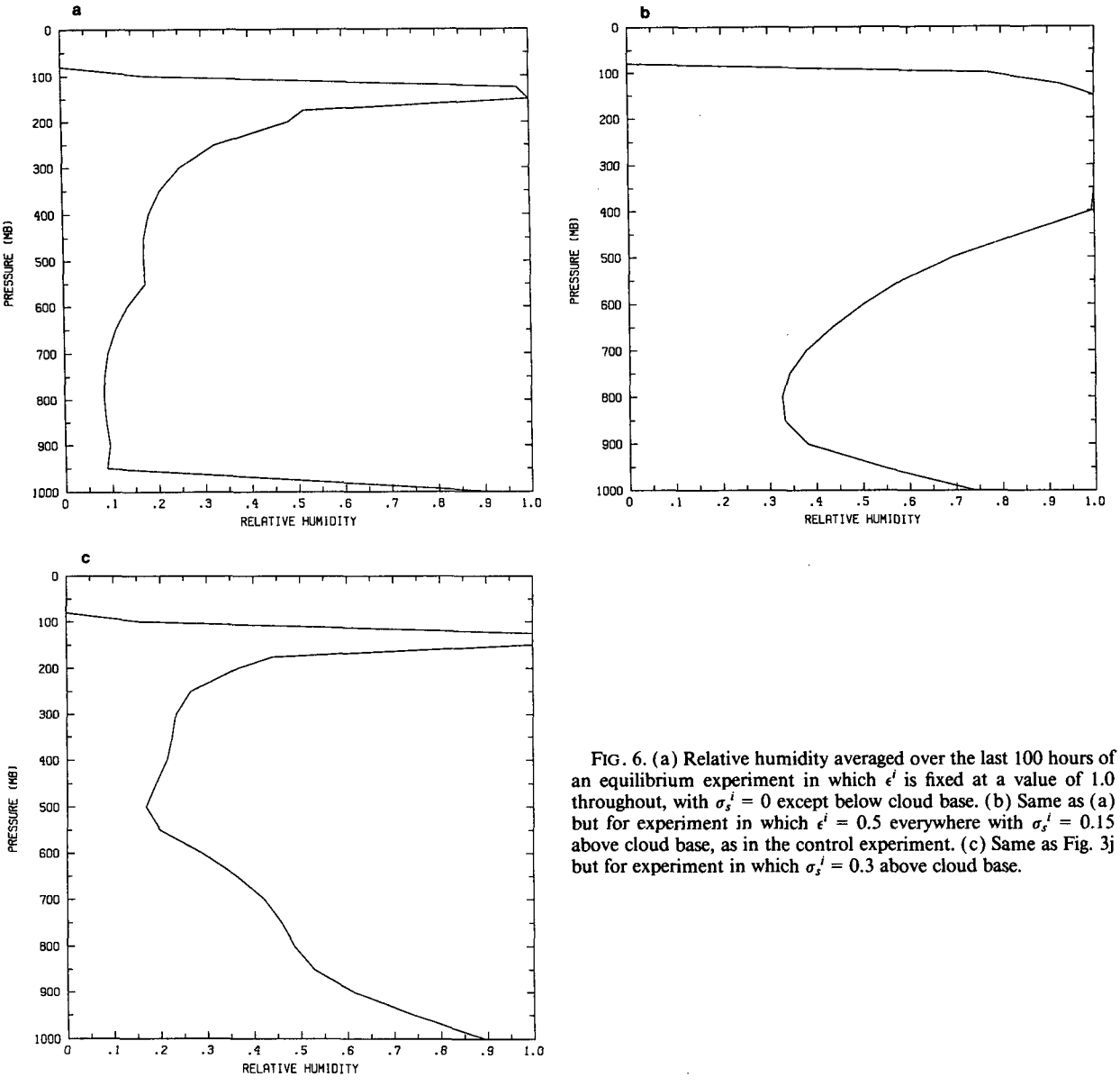

FIG. 6. (a) Relative humidity averaged over the last 100 hours of an equilibrium experiment in which ϵ^i is fixed at a value of 1.0 throughout, with $\sigma_s^i = 0$ except below cloud base. (b) Same as (a) but for experiment in which $\epsilon^i = 0.5$ everywhere with $\sigma_s^i = 0.15$ above cloud base, as in the control experiment. (c) Same as Fig. 3j but for experiment in which $\sigma_s^i = 0.3$ above cloud base.

no water is supplied at the top boundary. The profiles of warming and cooling (Fig. 8c) show that above the inversion radiative cooling balances large-scale subsidence warming. The excess large-scale subsidence warming at the trade inversion is balanced by the cooling due to net negative convective mass fluxes by penetrative downdrafts. (Alternatively, this cooling may be interpreted as resulting from evaporation at the tops of trade cumuli.) In the lower troposphere, the radiative cooling balances net upward mass flux in convective updrafts near cloud base. Radiative cooling balances warming by subsidence into the subcloud layer.

The water balance (Fig. 8d) shows that the drying due to large-scale subsidence through the inversion is balanced by net moistening due to the trade cumuli. The drying of the boundary layer by the convection is balanced by surface evaporation. The buoyancy of reversibly lifted subcloud air (Fig. 8e) reaches almost 2.0°C at 800 mb, where the relative humidity peaks at 89% (Fig. 8b). The mass flux profiles (Fig. 8f) show that the convective clouds are just deep enough (given my specification of ϵ^i) to allow for light precipitation, whose concentration peaks at about 0.1 g kg^{-1}. The profiles of entrainment and detrainment (Fig. 8g) show the entrainment into penetrative downdrafts near the trade inversion and the detrainment around 950–750 mb.

When the thermodynamic sounding is plotted on a θ_e–Q diagram (Fig. 8h) there is a nearly perfect mixing-line structure between cloud base ($\sim$14 g kg^{-1}) and the inversion. (The "line" between the surface and cloud base has data only at the two end points.)

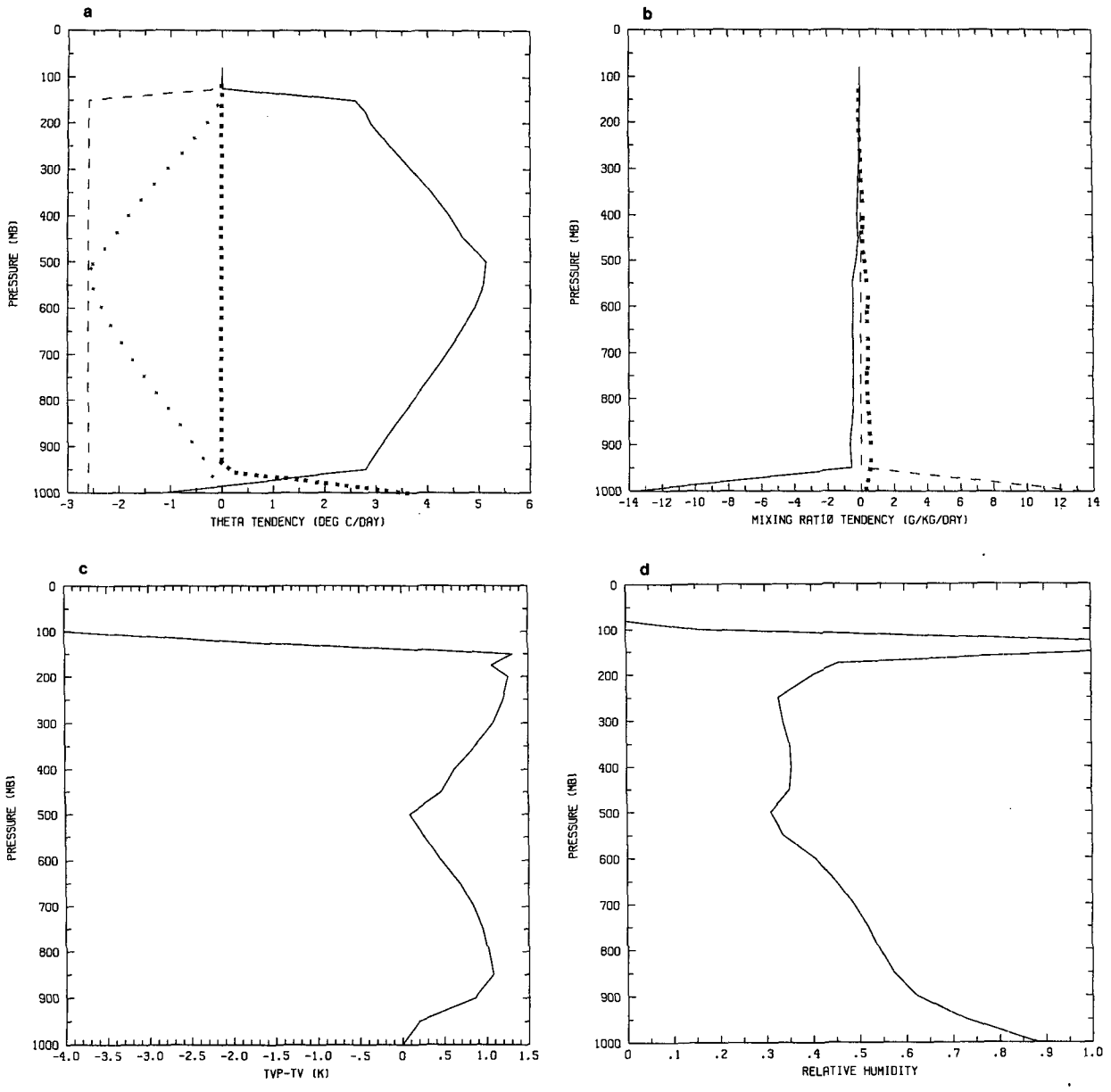

FIG. 7. Distributions of various quantities averaged over the last 100 hours of a simulation in which a parabolic distribution of upward motion, with a peak value of -30 mb day^{-1}, is imposed (see text). (a) convective and radiative heating, as in Fig. 3d, but with adiabatic cooling by imposed ascent shown by asterisks. (b) Convective water vapor tendency, as in Fig. 3e, but also showing moistening owing to imposed large-scale ascent. (c) Buoyancy, as in Fig. 3i. (d) Relative humidity (compare to Fig. 3j).

g. *Time-varying forcing*

An important characteristic of a convective representation is its ability to respond smoothly to changes in large-scale forcing. To test this feature of the present scheme, I apply (33) but with the quantity ω_m varying with time according to $\cos(\gamma t)$, with $\gamma = 1/(4 \text{ days})$. The amplitude of the imposed vertical velocity is again 30 mb day^{-1}. The running-mean precipitation (Fig. 9) demonstrates that the precipitation tracks the vertical velocity with a lag of no more than a few hours. The budgets and fields averaged over a period are nearly identical to those of the control experiment. If the large-scale vertical velocity were free to respond to temperature perturbations, the conversion of potential to kinetic energy over a wave period would be

$$\text{CPK} = -\frac{R}{g}\int_0^P \int_{p_t}^{p_0} \omega T \frac{dp}{p}\, dt$$

where R is the gas constant and P is the period of the large-scale motion. In this experiment, CPK is slightly negative, indicating that convection is attempting to damp the imposed large-scale motion.

5. Comparison with existing convection representations

The main difference between the present scheme and most other existing representations is that the former regards the subcloud-scale updrafts and downdrafts, rather than clouds themselves, as the main agents of convective transport. I have attempted as much as possible to mimic the physics of these drafts as elucidated by the observations described in section 2. The main features of the saturated drafts include reversible ascent, mixing with the environment, and transport to a level at which further mixing would result in zero buoyancy. In addition to the penetrative downdrafts, the falling precipitation drives an unsaturated downdraft similar in concept to the model of Brown (1979) and to that assumed by Nitta (1977) in his diagnostic study.

With respect to the buoyancy sorting of subcloud-scale elements, this scheme is most similar to that of Raymond and Blyth (1986), except that it includes precipitation.

The main problem in representing cumulus convection is to account for the redistribution of water, including its net fallout as precipitation. This is ultimately a microphysical and cloud dynamical question, as pointed out by Ooyama (1971), and such details cannot be ignored. The present scheme requires the specification, or relation to other model parameters, of two important sets of parameters: the parcel precipitation efficiencies (ϵ^i) and the fraction ($\sigma_s{}^i$) of precipitation that falls into unsaturated air. In addition, there is a weak dependence on the parameter σ_d, the assumed fractional area covered by the unsaturated downdraft. The evaporation of precipitation is calculated from a bulk formula. The mass flux of individual updrafts is calculated from the available energy for buoyant ascent and time-dependent fractional areas, but in quasi-equilibrium conditions it is, in practice, determined by the environmental forcing; downdraft mass fluxes follow from the updrafts.

No attempt at exhaustive comparisons will be made here, but a brief survey of other schemes follows.

The earliest attempts to account for convection in general circulation models were made by Manabe et al. (1965) and Miyakoda et al. (1969). Their schemes are referred to as moist convective adjustment. When properly viewed, these schemes are not actual representations of the ensemble effects of unresolved clouds, but rather are convective adjustments within explicitly resolved clouds. These adjustments prevent the explicit clouds from being *locally* unstable to small vertical displacements within the explicit clouds. The adjustment proceeds exactly as in dry convective adjustment, as described in the Introduction, but θ_e is used as the conserved buoyancy variable. The final state is assumed to be saturated in the fraction of grid box assumed to contain cloud, and all condensed water is removed as precipitation. In some ways, this adjustment is less arbitrary than dry convective adjustment since the final moisture distribution is constrained by the Clausius–Clapeyron relation in the former case.

It is important to note that models employing "hard" convective adjustment cannot release instability until and unless the explicitly resolved atmosphere becomes saturated,[1] and then only in the layer that is saturated. The large-scale model literally forms its own clouds; the adjustment only ensures that they are internally stable. Since an explicit humidity threshold must be reached for the adjustment to proceed, large CAPE can and does build up in the model atmosphere where it is unsaturated. For purposes of calculating the radiative effects of water vapor, convective adjustment, whether "hard" or "soft," produces some grid points or assumed fractions of grid boxes that are saturated, while the other grid points or fractions of grid boxes are too dry, because no condensed water is detrained from clouds. When averaged over many grid points in the "hard" case, or over a grid box in the "soft" case, it is not clear whether the relative humidity will be too large or too small, but there is little basis for believing that it will be correct.

An important variant on convective adjustment was introduced by Betts (1986). Unlike "hard" adjustment, Betts' scheme does not require explicit saturation but operates when and only when the large scale is unstable to parcel ascent, as in the present scheme. In this sense, the Betts scheme is a proper representation of the ensemble effects of clouds. This scheme relaxes the atmosphere back toward empirically defined reference profiles of temperature and mixing ratio with a specified relaxation time. The profiles effectively determine both the vertically integrated heating (precipitation) and the profile of moistening, but the predictability of the temperature and water vapor profiles is severely limited by the imposed profiles. Moreover, there is little physical basis for the universality of the water vapor profile. The scheme described in this paper retains the predictability of the water vapor profile, but the temperature profile is strongly constrained toward a virtual moist adiabat, as in the Betts scheme.

A number of authors have also devised schemes that activate when and only when the large scale is unstable to parcel ascent. These include the schemes of Kurihara (1973), Kreitzberg and Perkey (1976), Fritsch and Chappell (1980), and Hansen et al. (1983). With the exception of the Hansen et al. scheme, all of these use an entraining plume model for the updraft; that is, the cloud is considered the main convecting entity. It is principally in this respect that these schemes depart from the present one, which abandons the entraining plume in favor of buoyancy sorting. The Fritsch and Chappell scheme and the Kreitzberg and Perkey scheme also have downdrafts, with the latter offering a particularly detailed description of the microphysics of collection and fall of condensed water. All the afore-

[1] In some applications, the threshold humidity is less than 100%.

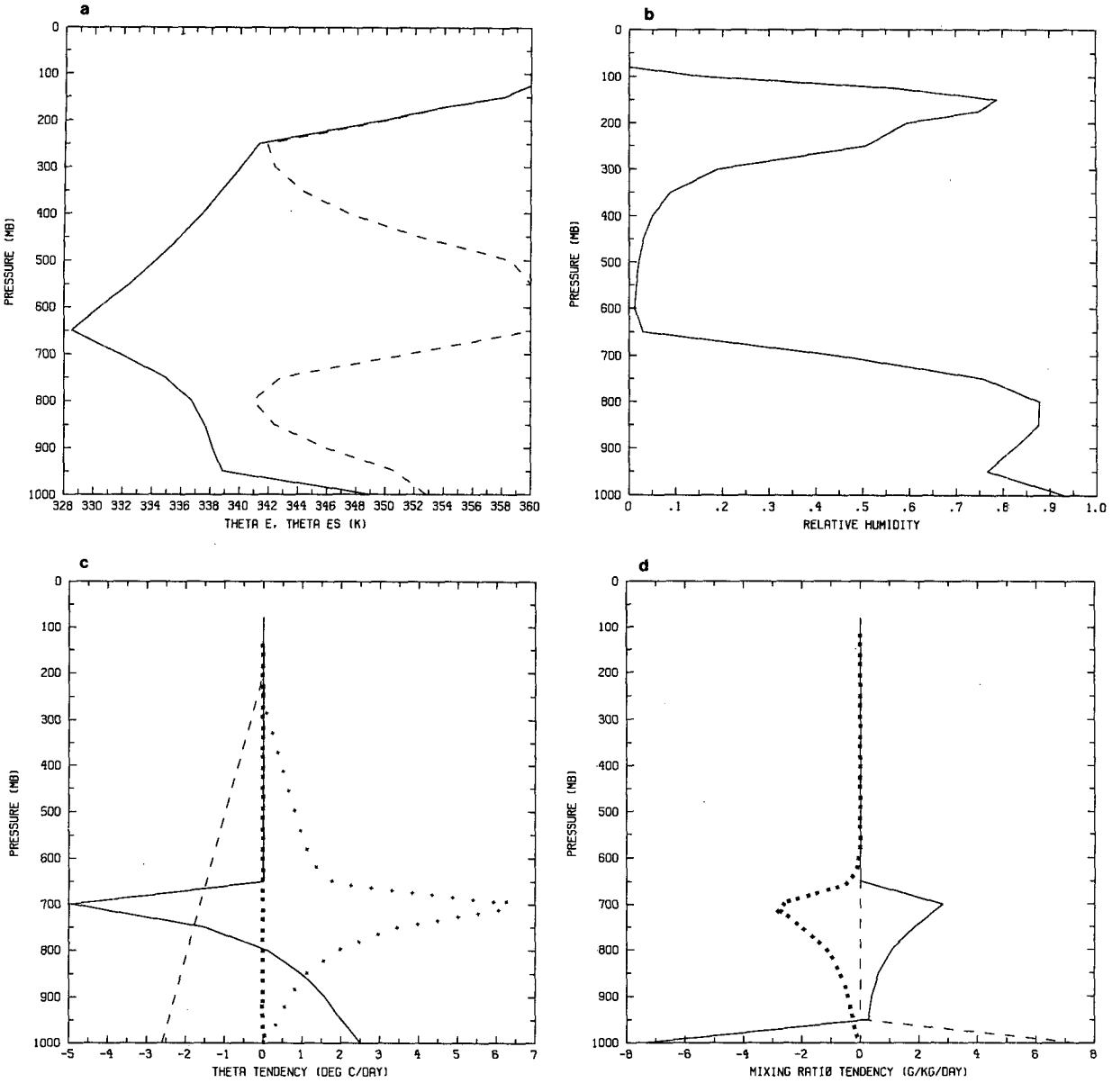

FIG. 8. Distributions of various quantities averaged over the last 100 hours of an experiment in which large-scale descent, with a peak value of 30 mb day^{-1}, is imposed (see text). (a) Equivalent potential temperature and saturated equivalent potential temperature, as in Fig. 3k. (b) Relative humidity (compare to Figs. 3j and 8d). (c) Heating, as in Fig. 7a. (d) Moistening, as in Fig. 7b.

mentioned schemes have somewhat different ways of calculating the cloud-base mass flux of updrafts, but as argued earlier in this paper, these differences should not affect the results of the schemes under quasi-equilibrium conditions in which the environmental forcing effectively determines the cloud-base mass flux, given only that the schemes turn on when the atmosphere is unstable to parcel ascent.

Among the most popular schemes are those in which the vertically integrated heating is constrained by the explicitly resolved convergence of water vapor. This was pioneered by Kuo (1965, 1974) and has been used as a constraint by Anthes (1977), Geleyn (1985), Tiedtke (1989), and others. A variant on this was made by Frank and Cohen (1987), who employed mass, rather than moisture, convergence. A wide variety of methods has been employed to determine the partitioning between moistening and precipitation and the vertical distributions of heating and moistening.

There are a number of serious drawbacks to such schemes, aside from problems related to the details of the cloud models used. In essence, a sound diagnostic relationship has been turned into a causal relationship with no justification. The results can be unphysical; for example, conditional instability can accumulate in the absence of moisture convergence and evaporation,

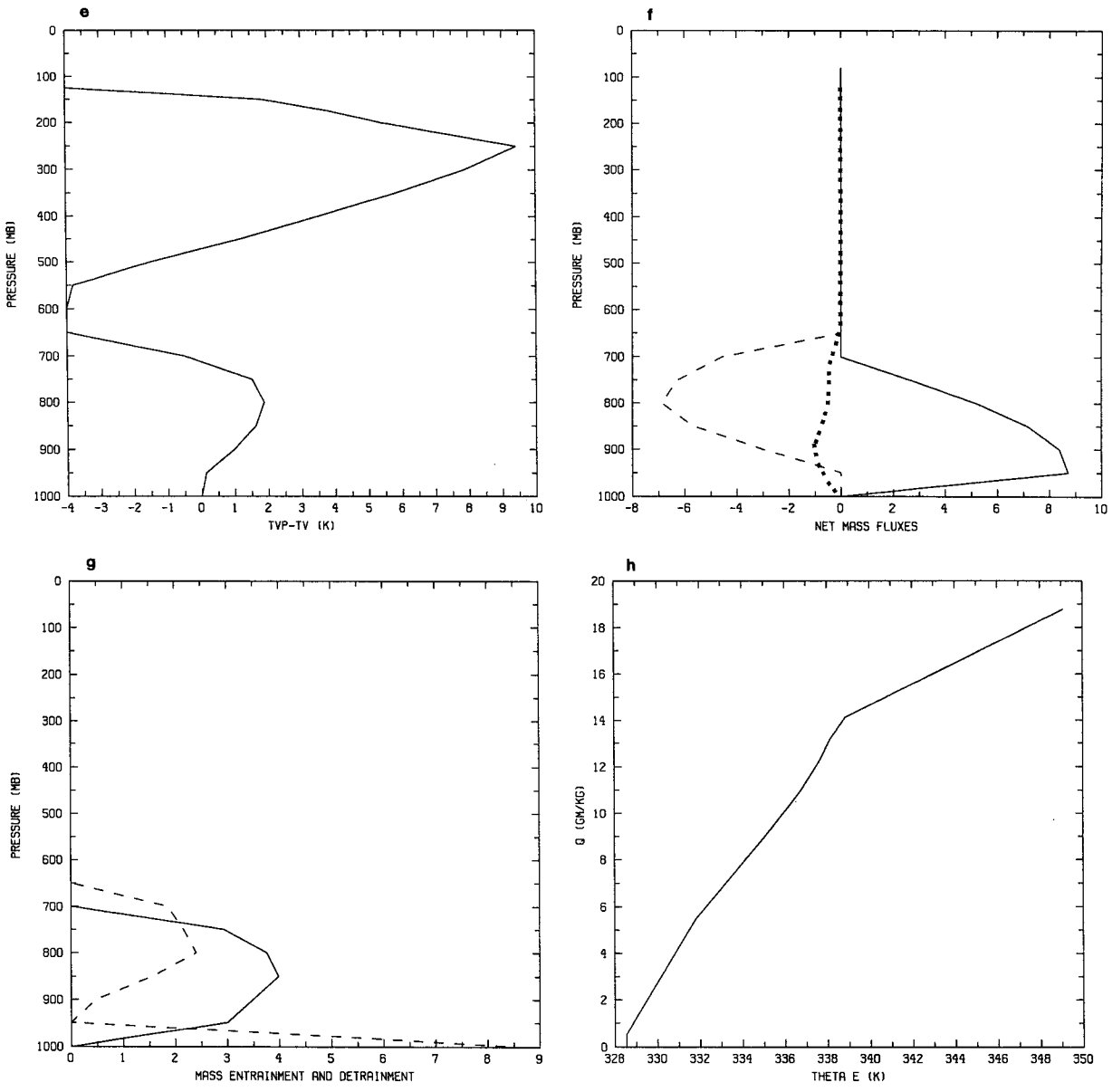

FIG. 8. (*Continued*) (e) Buoyancy, as in Fig. 7c. (f) Mass fluxes, as in Fig. 3f. (g) Entrainment and detrainment, as in Fig. 3g. (h) Mixing diagram, as in Fig. 3d.

resulting in large CAPE under conditions in which one would not normally expect it. Kuo-type schemes therefore share with moist convective adjustment an artificial restraint on the release of conditional instability. For these reasons, Kuo schemes and moist adjustment schemes are CISK-able, whereas other schemes, which do not promote artificial accumulation of CAPE, are less so, if at all.

Finally, there is the elegant scheme of Arakawa and Schubert (1974). The main virtue of this scheme lies in its determination of the spectrum of cloud-base mass fluxes by demanding that the convection dissipate instability at precisely the rate at which it is generated by resolved processes. This quasi-equilibrium assumption is supported by observations and by the results of schemes, such as the present one, that do not impose it. The arbitrary nature of the cloud-base mass flux in virtually all other schemes is thus absent in this case. The main drawbacks of this scheme, as originally formulated, are that it relies on an entraining plume model which, as has been already pointed out, is not supported by observations; it contains no downdrafts, and it cannot be expected to handle episodes of stored-energy convection. The absence of downdrafts was cited by Lord (1982) as a reason why semiprognostic tests of the scheme produce too much warming and drying at low levels. Cheng and Arakawa (1990) have recently produced a revision of the original Arakawa and

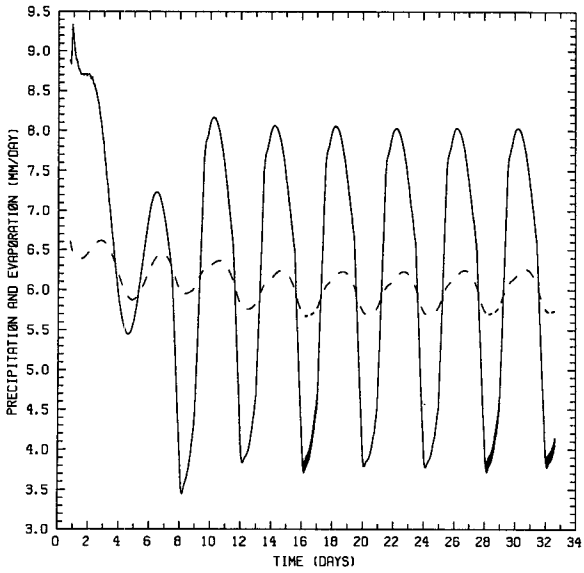

FIG. 9. Precipitation and evaporation, as in Fig. 3a, except with an imposed vertical velocity of magnitude 30 mb day varying sinusoidally over a 4-day period (see text).

Schubert scheme that incorporates downdrafts; this appears to be a significant improvement.

6. Conclusions

The representation of cumulus convection described in this paper is based as much as possible on the dynamics and microphysics of convection as revealed by recent detailed aircraft observations. These observations suggest that an idealization of the convective process based on reversible ascent of subcloud-scale entities, mixing, and buoyancy sorting (similar to the concept of Raymond and Blyth 1986) is better than the oft-employed idealization based on bulk-entraining plumes (Kurihara 1973; Kreitzberg and Perkey 1976; Fritsch and Chappell 1980; Arakawa and Schubert 1974; Frank and Cohen 1987; Tiedtke 1989). I have argued that the main problems that must be dealt with are the determination of how much condensed water ultimately falls out as rain, which governs the net heating, and the vertical distribution of moistening, both of which depend on the details of cloud dynamical and microphysical parameters. The main parameters of the present scheme are closely tied to these processes. They are the parcel precipitation efficiencies (ϵ^i), which govern how much condensed water in a given parcel is converted to precipitation, and the parameters $\sigma_s{}^i$, which determine how much precipitation falls back through cloudy air as opposed to environmental air. The vertical profiles of relative humidity that result from equilibrium convection are quite sensitive to these parameters, as indeed nature must be sensitive to the details of how condensed water is converted into precipitation.

A great deal of effort has been expended in the past on determining the factors that govern the mass flux into cumulus cloud bases. These efforts have resulted in the imposition of various constraints on the mass flux, including moisture convergence (Kuo-type schemes), mass convergence (Frank and Cohen 1987), and constraints based on the rate of release of conditional instability (Kreitzberg and Perkey 1976; Fritsch and Chappell 1980; Hansen et al. 1983; Betts 1986). I argue, in contrast, that provided one is not concerned with explicitly simulating mesoscale convective systems, the exact specification of the mass fluxes is superfluous as long as the fluxes are in some measure controlled by parcel instability, because in practice the mass fluxes will be determined by the environmental forcing, i.e., by quasi-equilibrium. This constraint was imposed explicitly by Arakawa and Schubert (1974). The present work demonstrates this point clearly through experiments in which the fractional areas covered by convective drafts are fixed. Even when these fixed areas are varied over an order of magnitude, the resulting thermodynamic profiles are very similar to those of the control run. Even in a one-dimensional model such as the one used here, the environment can control the mass flux by controlling both the degree of parcel instability and the frequency of convection; in higher-dimensional models one might expect the additional degrees of freedom to come into play as well. Naturally, these arguments do not apply to stored energy convection of the kind experienced occasionally in middle latitudes (particularly North America); here the rate at which stored energy is released becomes an important consideration.

Validation of this and other representations of convection involves several subtleties. A possible method would involve the specification of the initial vertical distributions of temperature and water vapor and the time evolutions of vertical motion, radiative cooling, and surface fluxes (but not water vapor fields) in a small-scale array such as the GATE A/B ship array; the schemes would then be validated by their ability to predict the time evolution of the vertical distributions of relative humidity—the most sensitive predictand. Such tests are underway and will be reported in the near future.

Acknowledgments. This research is supported by the National Science Foundation under Grant ATM-8818472. The author thanks Joel Sloman for typing the manuscript.

REFERENCES

Anthes, R. A., 1977: A cumulus parameterization scheme utilizing a one-dimensional cloud model. *Mon. Wea. Rev.*, **105**, 270–286.

Arakawa, A., and W. H. Schubert, 1974: Interaction of a cumulus cloud ensemble with the large-scale environment. Part I. *J. Atmos. Sci.*, **31**, 674–701.

Betts, A. K., 1982: Saturation point analysis of moist convective overturning. *J. Atmos. Sci.*, **39,** 1484–1505.

——, 1986: A new convective adjustment scheme. Part I: Observational and theoretical basis. *Quart. J. Roy. Meteor. Soc.*, **112,** 677–691.

——, and B. A. Albrecht, 1987: Conserved variable analysis of the convective boundary layer thermodynamic structure over the tropical oceans. *J. Atmos. Sci.*, **44,** 83–99.

Blyth, A. M., W. A. Cooper and J. B. Jensen, 1988: A study of the source of entrained air in Montana cumuli. *J. Atmos. Sci.*, **45,** 3944–3964.

Boatman, J. F., and A. H. Auer, 1983: The role of cloudtop entrainment in cumulus clouds. *J. Atmos. Sci.*, **40,** 1517–1534.

Brown, J. M., 1979: Mesoscale unsaturated downdrafts driven by rainfall evaporation: A numerical study. *J. Atmos. Sci.*, **36,** 313–338.

Cheng, M.-D., and A. Arakawa, 1990: Inclusion of convective downdrafts in the Arakawa-Schubert cumulus parameterization. Tech. Rep., Dept. of Atmospheric Science, University of California at Los Angeles, 69 pp.

Emanuel, K. A., 1981: A similarity theory for unsaturated downdrafts within clouds. *J. Atmos. Sci.*, **38,** 1541–1557.

——, 1989: The finite-amplitude nature of tropical cyclogenesis. *J. Atmos. Sci.*, **46,** 3431–3456.

Frank, W. M., and C. Cohen, 1987: Simulation of tropical convective systems. Part I: A cumulus parameterization. *J. Atmos. Sci.*, **44,** 3787–3799.

Fritsch, J. M., and C. F. Chappell, 1980: Numerical prediction of convectively driven mesoscale pressure systems. Part I: Convective parameterization. *J. Atmos. Sci.*, **37,** 1722–1733.

Geleyn, J.-F., 1985: On a simple, parameter-free partition between moistening and precipitation in the Kuo scheme. *Mon. Wea. Rev.*, **113,** 405–408.

Hansen, J., G. Russell, D. Rind, P. Stone, A. Lacis, S. Lebedeff, R. Ruedy and L. Travis, 1983: Efficient three-dimensional global models for climate studies. Models I and II. *Mon. Wea. Rev.*, **111,** 609–662.

Houze, R. A., Jr., 1977: Structure and dynamics of a tropical squall-line over Oklahoma. *Mon. Wea. Rev.*, **105,** 1540–1567.

——, 1982: Cloud clusters and large-scale vertical motions in the tropics. *J. Meteor. Soc. Japan,* **60,** 396–410.

——, 1988: Convective and stratiform precipitation in the tropics. *Proc., Int. Symp. on Tropical Precipitation Measurements.* Tokyo, Science and Technology Corp.

——, 1989: Observed structure of mesoscale convective systems and implications for large-scale heating. *Quart. J. Roy. Meteor. Soc.*, **115,** 425–462.

Jensen, J. B., P. H. Austin, M. B. Baker and A. M. Blyth, 1985: Turbulent mixing, spectral evolution and dynamics in a warm cumulus cloud. *J. Atmos. Sci.*, **42,** 173–192.

Johnson, R. H., 1984: Partitioning tropical heat and moisture budgets into cumulus and mesoscale components: Implications for cumulus parameterization. *Mon. Wea. Rev.*, **112,** 1590–1601.

Klemp, J. B., and R. B. Wilhelmson, 1978: The simulation of three-dimensional convective storm dynamics. *J. Atmos. Sci.*, **35,** 1070–1096.

Kreitzberg, C. W., and D. J. Perkey, 1976: Release of potential instability: Part I. A. sequential plume model within a hydrostatic primitive equation model. *J. Atmos. Sci.*, **33,** 456–475.

Kuo, H.-L., 1965: On formation and intensification of tropical cyclones through latent heat release by cumulus convection. *J. Atmos. Sci.*, **22,** 40–63.

——, 1974: Further studies of the parameterization of the influence of cumulus convection on large-scale flow. *J. Atmos. Sci.*, **31,** 1232–1240.

Kurihara, Y., 1973: A scheme of moist convective adjustment. *Mon. Wea. Rev.*, **101,** 547–553.

LaMontagne, R. G., and J. W. Telford, 1983: Cloud top mixing in small cumuli. *J. Atmos. Sci.*, **40,** 2148–2156.

LeMone, M. A., G. M. Barnes, E. J. Szoke and E. J. Zipser, 1984: The tilt of the leading edge of mesoscale tropical convective lines. *Mon. Wea. Rev.*, **112,** 510–519.

Lindzen, R. S., 1990: Some coolness concerning global warming. *Bull. Amer. Meteor. Soc.*, **71,** 288–299.

Lord, S. J., 1982: Interaction of a cumulus cloud ensemble with the large-scale environment. Part III: Semiprognostic test of the Arakawa-Schubert cumulus parameterization. *J. Atmos. Sci.*, **39,** 88–103.

Malkus, J. S., 1954: Some results of a trade-cumulus cloud investigation. *J. Meteor.*, **11,** 220–237.

Manabe, S., J. Smagorinsky and R. F. Strickler, 1965: Simulated climatology of a general circulation model with a hydrologic cycle. *Mon. Wea. Rev.*, **93,** 769–798.

Miyakoda, K., J. Smagorinsky, R. F. Strickler and G. D. Hembree, 1969: Experimental extended predictions with a nine-level hemispheric model. *Mon. Wea. Rev.*, **97,** 1–76.

Nitta, T., 1977: Response of cumulus updraft and downdraft to GATE A/B-scale motion systems. *J. Atmos. Sci.*, **34,** 1163–1186.

Ogura, Y., and T. Takahashi, 1971: Numerical simulation of the life cycle of a thunderstorm cell. *Mon. Wea. Rev.*, **99,** 845–911.

Ooyama, K., 1971: A theory on parameterization of cumulus convection. *J. Meteor. Soc. Japan,* **49,** (Special issue), 744–756.

Paluch, I. R., 1979: The entrainment mechanism in Colorado cumuli. *J. Atmos. Sci.*, **36,** 2462–2478.

Raga, G. B., J. B. Jensen and M. B. Baker, 1990: Characteristics of cumulus cloud bands off the coast of Hawaii. *J. Atmos. Sci.*, **47,** 338–355.

Raymond, D. J., 1979: A two-scale model of moist, nonprecipitating convection. *J. Atmos. Sci.*, **36,** 816–831.

——, and M. H. Wilkening, 1982: Flow and mixing in New Mexico mountain cumuli. *J. Atmos. Sci.*, **39,** 2211–2228.

——, and ——, 1985: Characteristics of mountain-induced thunderstorms and cumulus congestus clouds from budget measurements. *J. Atmos. Sci.*, **42,** 773–783.

——, and A. M. Blyth, 1986: A stochastic model for nonprecipitating cumulus clouds. *J. Atmos. Sci.*, **43,** 2708–2718.

Rotunno, R., J. B. Klemp and M. L. Weisman, 1988: A theory for strong, long-lived squall lines. *J. Atmos. Sci.*, **45,** 463–485.

Seitter, K. L., and H.-L. Kuo, 1983: The dynamical structure of squall-line type thunderstorms. *J. Atmos. Sci.*, **40,** 2932–2854.

Squires, P., 1958: Penetrative downdraughts in cumuli. *Tellus,* **10,** 382–389.

Stommel, H., 1947: Entrainment of air into a cumulus cloud. *J. Meteor.*, **4,** 91–94.

Taylor, G. R., and M. B. Baker, 1991: Entrainment and detrainment in cumulus clouds. *J. Atmos. Sci.*, **48,** 112–121.

Telford, J. W., 1975: Turbulence, entrainment and mixing in cloud dynamics. *Pure Appl. Geophys.*, **113,** 1067–1084.

Tiedtke, M., 1989: A comprehensive mass flux scheme for cumulus parameterization in large-scale models. *Quart. J. Roy. Meteor. Soc.*, **117,** 1779–1800.

Warner, J., 1955: The water content of cumuliform cloud. *Tellus,* **7,** 449–457.

——, 1970: On steady state one-dimensional models of cumulus convection. *J. Atmos. Sci.*, **27,** 1035–1040.

——, and P. Squires, 1958: Liquid water content and the adiabatic model of cumulus development. *Tellus,* **10,** 390–394.

Xu, K., and K. A. Emanuel, 1988: Is the tropical atmosphere conditionally unstable? *Mon. Wea. Rev.*, **117,** 1471–1479.

Zipser, E. J., 1969: The role of organized unsaturated convective downdraughts in the structure and rapid decay of an equatorial disturbance. *J. Appl. Meteor.*, **8,** 799–814.